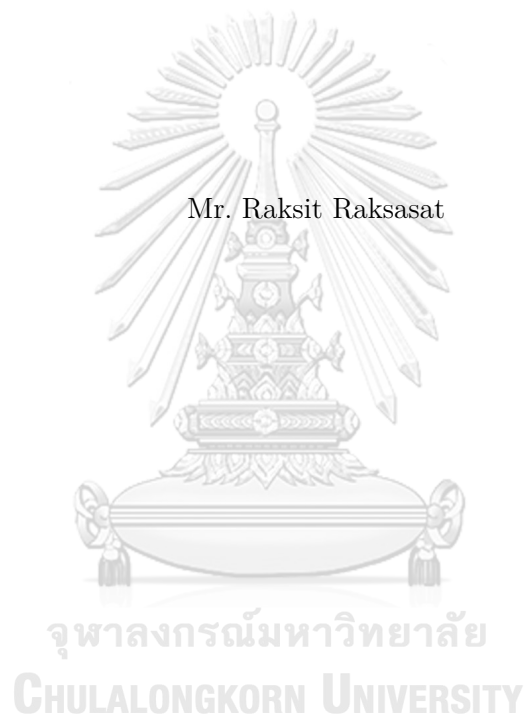


ACCURATE SURFACE ULTRAVIOLET RADIATION FORECASTING FOR
CLINICAL APPLICATIONS WITH DEEP NEURAL NETWORK

Mr. Raksit Raksasat



A Thesis Submitted in Partial Fulfillment of the Requirements
for the Degree of Master of Engineering in Computer Engineering

Department of Computer Engineering

FACULTY OF ENGINEERING

Chulalongkorn University

Academic Year 2020

Copyright of Chulalongkorn University

โมเดลทำนายรังสีอัลตราไวโอเล็ตในระดับพื้นผิวโลกที่มีความแม่นยำสูงเพื่อการประยุกต์ใช้ในการ
รักษาด้วยการเรียนรู้เชิงลึก



วิทยานิพนธ์นี้เป็นส่วนหนึ่งของการศึกษาตามหลักสูตรปริญญาวิศวกรรมศาสตรมหาบัณฑิต

สาขาวิชาวิศวกรรมคอมพิวเตอร์ ภาควิชาวิศวกรรมคอมพิวเตอร์

คณะวิศวกรรมศาสตร์ จุฬาลงกรณ์มหาวิทยาลัย

ปีการศึกษา 2563

ลิขสิทธิ์ของจุฬาลงกรณ์มหาวิทยาลัย

Thesis Proposal Title ACCURATE SURFACE ULTRAVIOLET RADIATION
FORECASTING FOR CLINICAL APPLICATIONS WITH
DEEP NEURAL NETWORK

By Mr. Raksit Raksasat

Field of Study Computer Engineering

Thesis Advisor Ekapol Chuangsuwanich, Ph.D.

Thesis Co-advisor Sira Sriswasdi, Ph.D.

Accepted by the FACULTY OF ENGINEERING, Chulalongkorn University in Partial Fulfillment of the Requirements for the Master of Engineering

..... Dean of the FACULTY OF
ENGINEERING
(Prof. Supot Teachavorasinskun, D.Eng.)

THESIS PROPOSAL COMMITTEE

..... Chairman
(Duangdao Wichadakul, Ph.D.)

..... Thesis Advisor
(Ekapol Chuangsuwanich, Ph.D.)

..... Thesis Co-advisor
(Sira Sriswasdi, Ph.D.)

..... External Examiner
(Sumaman Buntoung, Ph.D.)

CHULALONGKORN UNIVERSITY

รักษิต รักษาสัตย์: โมเดลทำนายรังสีอัลตราไวโอเล็ตในระดับพื้นผิวโลกที่มีความแม่นยำสูงเพื่อการประยุกต์ใช้ในการรักษาด้วยการเรียนรู้เชิงลึก. (ACCURATE SURFACE ULTRAVIOLET RADIATION FORECASTING FOR CLINICAL APPLICATIONS WITH DEEP NEURAL NETWORK) อ.ที่ปรึกษาวิทยานิพนธ์หลัก : ดร. เอกพล ช่วงสุนิช, อ.ที่ปรึกษาวิทยานิพนธ์ร่วม : ดร. สิริระ ศรีสวัสดิ์ 57 หน้า.

การได้รับปริมาณรังสีอัลตราไวโอเล็ตอย่างเหมาะสมให้ผลดีอย่างมากกับการรักษาสุขภาพและการรักษาทางการแพทย์ซึ่งรวมไปถึงการรักษาโรคสะเก็ดเงิน โดยปกติแล้วตู้อาบที่ใช้ในการรักษาด้วยแสงในโรงพยาบาลนั้นจะประกอบไปด้วยหลอดไฟสำหรับฉายแสงเทียมซึ่งสามารถปล่อยรังสีอัลตราไวโอเล็ตบีในความยาวคลื่นแถบความถี่กว้าง (ความยาวคลื่นหลักที่ปล่อย 280-360 นาโนเมตร, สูงสุดที่ 320 นาโนเมตร) หรือแถบความถี่สั้น (ความยาวคลื่นหลักที่ปล่อย 310-315 นาโนเมตร, สูงสุดที่ 311 นาโนเมตร) แต่สำหรับผู้ป่วยที่ไม่สามารถเข้าถึงศูนย์รักษาสำหรับการรักษาด้วยแสง การรักษาด้วยการอาบแดดหรือการรักษาด้วยแสงอาทิตย์เป็นอีกหนึ่งวิธีการรักษาที่ปลอดภัยและมีประสิทธิภาพ อย่างไรก็ตามเนื่องจากแสงอาทิตย์นั้นประกอบไปด้วยรังสีอัลตราไวโอเล็ตทุกความยาวคลื่น (290-400 นาโนเมตร) การอาบแดดจึงต้องทำอย่างระมัดระวังและต้องมีแพทย์ผิวหนังคอยให้คำปรึกษาโดยอิงจากการทำนายรังสีอัลตราไวโอเล็ตที่แม่นยำเพื่อลดโอกาสที่จะเกิดผลข้างเคียง ซึ่งในส่วนของการทำนายนั้น เราได้ใช้ข้อมูลรังสีอัลตราไวโอเล็ต 10 ปีที่เก็บรวบรวมจากนครปฐมในการสร้างโมเดลทำนายรังสีอัลตราไวโอเล็ตด้วยการเรียนรู้เชิงลึกที่มีความผิดพลาด 10% สำหรับการทำนายล่วงหน้า 24 ชั่วโมงและมีความผิดพลาดราว 13-16 % สำหรับการทำนายล่วงหน้า 7 วันถึง 4 สัปดาห์ ผลงานวิจัยนี้สามารถขยายไปใช้กับข้อมูลรังสีอัลตราไวโอเล็ตจากภูมิภาคทางภูมิศาสตร์ที่แตกต่างกันหรือมีความหลากหลายทางสเปกตรัมกิจกรรมทางชีวภาพ ผลงานวิจัยนี้จะเป็นหนึ่งในเครื่องมือสำคัญในการพัฒนาแผนการรักษาด้วยแสงอาทิตย์ในประเทศไทย โมเดลของเราสามารถเข้าถึงได้ทาง github.com/cmb-chula/SurfUVNVNet

ภาควิชา	วิศวกรรมคอมพิวเตอร์	ลายมือชื่อนิสิต
สาขาวิชา	วิศวกรรมคอมพิวเตอร์	ลายมือชื่ออ.ที่ปรึกษาหลัก
ปีการศึกษา	2563	ลายมือชื่อ.ที่ปรึกษาร่วม	

6270228721: MAJOR COMPUTER ENGINEERING

KEYWORDS: TYPESETTING / INTRODUCTION / LATEX

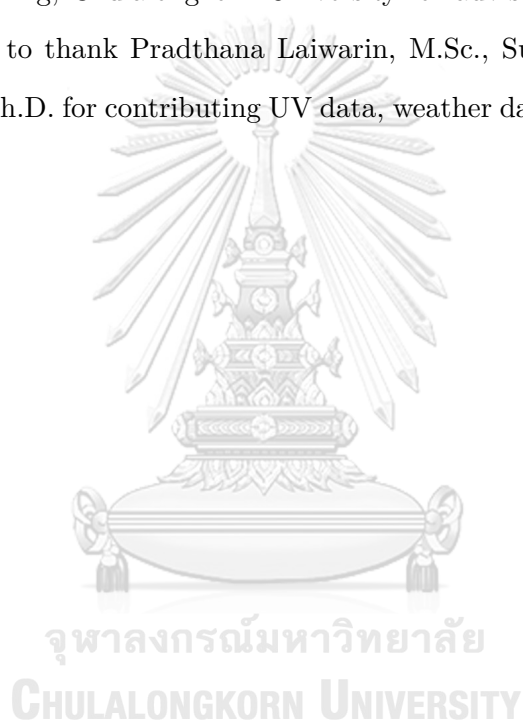
RAKSIT RAKSASAT : ACCURATE SURFACE ULTRAVIOLET RADIATION FORECASTING FOR CLINICAL APPLICATIONS WITH DEEP NEURAL NETWORK. ADVISOR : Ekapol Chuangsuwanich, Ph.D., THESIS COADVISOR : Sira Sriswasdi, Ph.D., 57 pp.

Exposure to appropriate doses of UV radiation provides enormously health and medical treatment benefits including psoriasis. Typical hospital-based phototherapy cabinets contain a bunch of artificial lamps, either broad-band (main emission spectrum 280-360 nm, maximum 320 nm), or narrow-band UV B irradiation (main emission spectrum 310-315nm, maximum 311nm). For patients who cannot access phototherapy centers, sun-bathing, or heliotherapy, can be a safe and effective treatment alternative. However, as sunlight contains the full range of UV radiation (290-400 nm), careful sun-bathing supervised by photodermatologist based on accurate UV radiation forecast is vital to minimize potential adverse effects. Here, using 10-year UV radiation data collected at Nakhon Pathom, Thailand, we developed a deep learning model for UV radiation prediction which achieves around 10% error for 24-hour forecast and 13-16% error for 7-day up to 4-week forecast. Our approach can be extended to UV data from different geographical regions as well as various biological action spectra. This will become one of the key tools for developing national heliotherapy protocol in Thailand. Our model has been made available at github.com/cmb-chula/SurfUVNet.

Department	: Computer Engineering	Student's Signature
Field of Study	: Computer Engineering	Advisor's Signature
Academic Year	: 2020	Co-advisor's signature

Acknowledgements

I would like to thank my thesis supervisor Ekapol Chuangsuwanich, Ph.D. and Sira Sriswasdi, Ph.D. for their assistance with a suggestion and Einapak Boontaveeyuwat, MD. and Jaruwan Pemcharoen, B.Sc. for evaluated the impact of UV forecast on heliotherapy planning. I also thank my project partner, Panyawut Sri-iesaranusorn from Faculty of Engineering, Chulalongkorn University for advising some methodology. Finally, I would like to thank Pradthana Laiwarin, M.Sc., Sumaman Buntoung, Ph.D., and Serm Janjai, Ph.D. for contributing UV data, weather data, and expertise in surface UV radiation.



CONTENTS

	Page
Abstract (Thai)	iv
Abstract (English)	v
Acknowledgements	vi
Contents	vii
List of Tables	x
List of Figures	xi
1 Introduction	1
1.1 Main contribution	3
1.2 Thesis overview	4
2 Background	5
2.1 Artificial Neural Network	5
2.2 Activation functions	5
2.2.1 Linear activation function	6
2.2.2 Sigmoid or Logistic activation function	6
2.2.3 Rectified linear unit (ReLU) activation function	6
2.2.4 Tanh activation function	6
2.2.5 Softmax activation function	7
2.3 Convolutional Neural Network	8
2.4 Recurrent Neural Network	8
2.5 Long Short Term Memory	9
2.5.1 Forget gate	9
2.5.2 Input gate	9
2.5.3 Output gate	10
2.6 Gated Recurrent Unit	10

2.6.1	Reset gate	11
2.6.2	Update gate	11
2.7	Encoder-Decoder Sequence to Sequence (Seq2Seq) model	11
3	Related Works	13
3.1	Modeling based on the physics of UV radiation	13
3.2	Hybrid between physics-based modeling and empirical techniques	14
3.3	Deep learning	14
4	Method	16
4.1	Surface UV and weather data acquisition	16
4.2	Data cleaning and preprocessing	17
4.3	SurfUVNet model architecture	19
4.3.1	Encoder	20
4.3.2	Decoder	20
4.4	Model training	21
5	Result	23
5.1	SurfUVNet model architecture	23
5.2	Benchmark procedure	24
5.3	Next-day antipsoriatic irradiance forecast for Nakhon Pathom dataset	25
5.4	Next-day downward solar UV irradiance forecast for Tokyo and London datasets	25
5.5	Adding weather information does not improve forecasting	28
5.6	Long-term antipsoriatic irradiance forecasting	32
6	Discussion	35
7	Conclusion	38
7.1	Summary	38
7.2	Future work	38
7.2.1	Adding attention mechanism to the model	38
7.2.2	Improving prediction for days with irregular UV profiles	39

References 40

BIOGRAPHY 46



จุฬาลงกรณ์มหาวิทยาลัย
CHULALONGKORN UNIVERSITY

LIST OF TABLES

Table	Page
5.1 Mean absolute percentage errors (MAPE) of the next-day antipsoriatic irradiance forecasting produced by SurfUVNet and benchmark models.	27
5.2 Mean absolute percentage errors (MAPE) of the next-day antipsoriatic irradiance forecasting produced by SurfUVNet and other models on the ERA5 Tokyo and London datasets.	29
5.3 Mean absolute percentage errors (MAPE) for long-term antipsoriatic irradiance forecasting for up to 28 days into the future on Nakhon Pathom dataset. 34	



LIST OF FIGURES

Figure	Page
2.1 Activation functions	7
2.2 Encoder-Decoder sequence-to-sequence (Seq2Seq) model architecture	12
4.1 Characteristics of UV and weather conditions at Nakhon Pathom, Thailand.	17
4.2 Schematic of SurfUVNet.	22
5.1 SurfUVNet accurately forecast antipsoriatic irradiance throughout the day	26
5.2 Characteristics of UV and weather conditions at Tokyo, Japan and London, England.	28
5.3 The distribution of cloud coverage in ERA5 validation and test sets.	29
5.4 SurfUVNet's forecast error weakly correlates with cloud coverage	31
5.5 Comparison of SurfUVNet performance with and without ozone and AOD500 as input	32
5.6 Long-term antipsoriatic irradiance forecasting	33

Chapter I

INTRODUCTION

Phototherapy using artificial light sources is one of the standard treatments for various skin conditions (Menter et al., 2010; Legat, 2018; Patrizi et al., 2017). With established national guidelines and standard dosimetry protocols, hospital-based phototherapy provides safe and effective treatment for a wide variety of patients. However, many skin patients in Thailand still lack access to hospital-based phototherapy due to the limited number of phototherapy centers as well as shortage of qualified phototherapy practitioners across the country. Also, phototherapy for skin diseases such as psoriasis is a long-time treatment, skin patients would have to bath in narrowband UVB (311–313 nm) that was emitted from artificial UV light lamp and have to repeat this process several times. This process is difficult for some patients to travel to hospitals that have available tools or phototherapy centers. Heliotherapy can solve these problem by let the patients sun-bathing in any area and come to hospital only for report and take a guideline from physicians.

Heliotherapy, or phototherapy using natural sunlight, has been reported effective for treating diverse health issues (Metzger, 1926; Gardiner, 1915; Alpert, 2015) and skin conditions (Linser and Harnack, 1962; Buchholz, 1969; Körbler, 1967) since 1890s. Several clinical studies have also shown success outcomes of supervised heliotherapy in mostly European countries, including the Canary Islands, Spain, Helsinki, Finland and Davos, Switzerland (Hitomi et al., 2017; Snellman, 1992; Snellman et al., 1993b; Takada et al., 1977; Snellman et al., 1992, 1993a). Despite clear benefits of heliotherapy, a key issue that limits its effectiveness is the substantial variation in surface UV radiation throughout the year and time of day. Therefore, accurate estimates of UV radiation, in conjunction with treatment action spectrum and dosimetry, are essential for developing a safe and effective heliotherapy protocol in long-term use for a particular geographical region (Krzyściński et al., 2012, 2014; Moosa and Esterhuysen, 2010). To date, a few studies have explored the prospect of quantitative heliotherapy planning based on UV radiation

forecast(Krzyścin et al., 2012, 2015).

Prediction of surface UV radiation can roughly be categorized into three groups: physics-based modeling, a hybrid between the physics and empirical techniques, and deep learning. Physics-based approaches calculate the amount of solar UV radiation that arrives at a certain location on Earth at a certain time mainly based on the Earth-Sun distance and the thickness of the Earth's ozone layer(Krzyścin et al., 2015; Allaart et al., 2006; Leccese et al., 2018). This is also known as the clear-sky UV radiation. Then, to obtain the amount of radiation on the Earth's surface, the clear-sky estimates are multiplied by factors such as Cloud Modification Factor(Krzyścin et al., 2015; Sudhibrabha et al., 2006) to account for reflection and scattering of UV in the atmosphere. Hybrid approaches rely on Physics knowledge to define UV-related factors, such as total ozone column, zenith angle, and weather conditions, but incorporate numerical simulations and regressions to estimate the contribution of these factors to the amount of surface UV radiation in a data-driven manner(Sudhibrabha et al., 2006; Deo et al., 2017; Feister et al., 2011; Foyo-Moreno et al., 1999). In contrast, deep learning approaches attempt to predict surface UV radiation data directly from past observations with little to no constraint on how UV-related factors interact(Qing and Niu, 2018; Wang et al., 2018; Elminir et al., 2008; Jacovides et al., 2015) Although deep learning is effective for forecasting time series(Siami-Namini and Namin, 2018) because of its ability to learn complex non-linear relationship between the input and output data, it requires a large amount of data to train, lacks interpretability, and does not perform well on new datasets with different distributions. It is expected that deep learning model for UV forecasting needs to be retrained for each geographical region. Recent works in the energy domain have successfully utilized recurrent neural network (RNN)(Elman, 1990) architectures, such as Long Short-Term Memory (LSTM)(Hochreiter and Schmidhuber, 1997) and Gated Recurrent Unit (GRU)(Cho et al., 2014), to predict solar photovoltaic power production(Qing and Niu, 2018; Wang et al., 2018; Husein and Chung, 2019; Gensler et al., 2016; Huang et al., 2019).

Study of surface UV radiation in Thailand (Janjai et al., 2010; Buntoung et al., 2012) showed that this region has sufficient UV radiation year round, indicating that heliotherapy is a promising treatment alternative for skin patients in the country. This thesis studies and developed a deep learning model for surface UV radiation forecasting which has acceptance error range of 10-25% indicated in broadband UVB phototherapy guidelines worldwide (Menter et al., 2010; Nast et al., 2017). Our model is based on the encoder-decoder architecture (Sutskever et al., 2014) and 10-year surface UV radiation data collected at Nakhon Pathom, Thailand (13.82 N, 100.04 E) from 2009 to 2019, our work serves as a key step toward the establishment of the national heliotherapy protocol in Thailand.

1.1 Main contribution

The main contribution of this thesis can be summarized as follows:

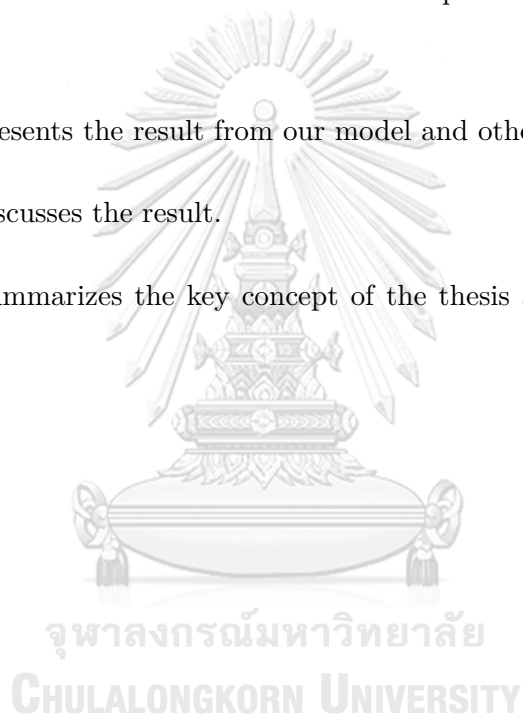
- Developed a deep neural network for surface UV radiation forecasting. Our model consistently achieves 10-25 MAPE, which is acceptable for clinical applications, when applied to data from multiple geographic regions.
- Our model uses only UV data as input. This would make our model applicable to regions where other climate data are unavailable.
- Our model also yields acceptance error range when making long-term forecast (7-day to 4-week).

This thesis proposes a complete pipeline for our UV forecasting model, including data preprocessing, model architecture, and parameter tuning.

1.2 Thesis overview

This thesis is organized as follows:

- Chapter 2 describes the background knowledge for building a deep neural network in time series prediction task.
- Chapter 3 reviews the work related to UV forecasting.
- Chapter 4 describes the model architecture and parameter setting for training the model.
- Chapter 5 presents the result from our model and other benchmark models.
- Chapter 6 discusses the result.
- Chapter 7 summarizes the key concept of the thesis and provides directions for future work.



Chapter II

BACKGROUND

This section explains the fundamentals of deep learning and deep learning techniques related to time series tasks. We also explain the encoder-decoder architecture which inspires our model design.

2.1 Artificial Neural Network

Artificial neural network (ANN) is a model that consists of many connected computation units called neurons that are arranged in various layers. Each artificial neuron resembles a biological neuron in our body which operates by passing signal values to neighboring neurons. Each connection between two neurons is specified with a weight parameter that is multiplied to the signal value passing through that connection. The input of an artificial neuron is the weighted sum of signal from other neurons plus a bias term. The output of the neuron is then subjected to a non-linear activation function to transform the signal. These processes repeat until the signal reaches the last layer, which produces an answer to the task. During the training process, the output from the last layer is compared to the ground truth target and the error is calculated by using a cost function, or loss function. The gradient of the loss function is then back-propagated (Rumelhart et al., 1986) through layers of the model to optimize the weight parameters to reduce the amount of errors made by the model.

2.2 Activation functions

Activation function is useful not only to limit the range of a neuron's output, such as from 0 to 1, but also to introduce some non-linearity, such as sigmoid transformation, that lets ANN solve complex problem. In this thesis, we explain the following activation functions that are used in general tasks: ReLU, sigmoid, tanh, and softmax.

2.2.1 Linear activation function

A linear activation function is a simple straight-line function as shown in Eq. 2.1 (Figure 2.1 a). An ANN with a linear activation function will behave like a simple linear regression mode and typically cannot fit complex, real-world data.

$$F(x) = ax \quad (2.1)$$

2.2.2 Sigmoid or Logistic activation function

Sigmoid is a popular activation function that is mostly used in last layer for predicting probability value because the output of sigmoid function lies in the interval $(0, 1)$. The sigmoid function is shown in Eq. 2.2 (Figure 2.1 b).

$$\sigma(x) = \frac{1}{1 + e^{-x}} \quad (2.2)$$

2.2.3 Rectified linear unit (ReLU) activation function

ReLU is a piece-wise linear function that has been shown to perform well in many networks. The output from ReLU is zero if the input is negative and equal to the identify function otherwise, as shown in Eq. 2.3 (Figure 2.1 c). This allows some neurons to be deactivated if they produce negative output values.

$$ReLU(x) = \max(0, x) \quad (2.3)$$

2.2.4 Tanh activation function

Tanh or hyperbolic tangent activation function is similar in shape to sigmoid but its range is the interval $(-1, 1)$ and it is zero-centered, as shown in Eq. 2.4 (Figure 2.1

d). The advantage of tanh function is that it supports negative output value.

$$\text{Tanh}(x) = 2\sigma(2x) - 1 \quad (2.4)$$

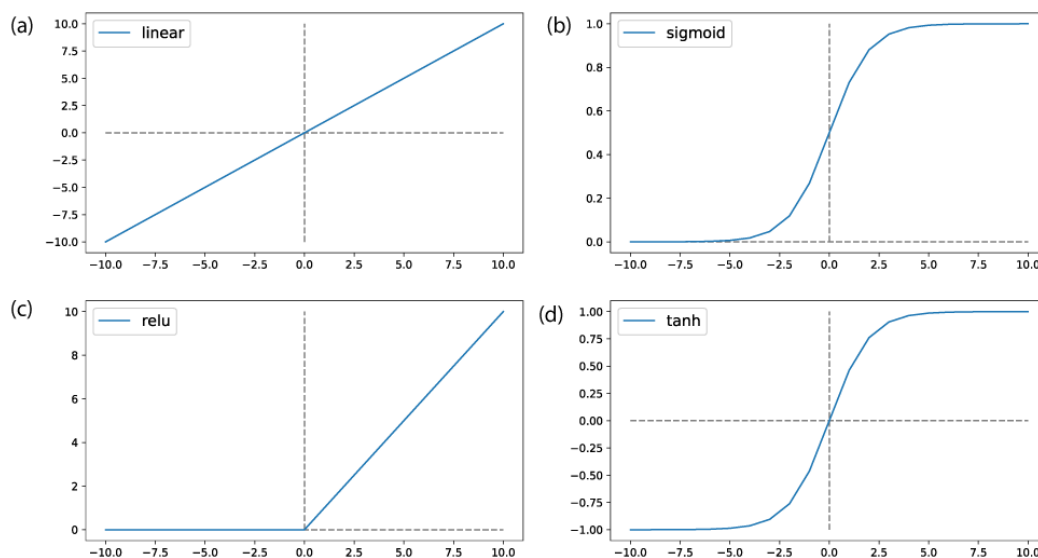


Figure 2.1: **Activation functions** (a) Linear function multiplies the input by a constant. (b) Sigmoid function transforms the input into the range from 0 to 1. (c) ReLU function returns zero when the input is negative and behaves as an identity function otherwise. (d) Tanh function outputs values in the range from -1 and 1.

2.2.5 Softmax activation function

Softmax is used in multi-class classification task because it transforms the outputs to make them sum to one. The behaviour lets us interpret the output of softmax as the probability distribution among classes. The equation of softmax is shown in Eq. 2.5.

$$\text{softmax}(x_i) = \frac{\exp(x_i)}{\sum_j \exp(x_j)} \quad (2.5)$$

2.3 Convolutional Neural Network

Convolutional Neural Network (CNN) (Lecun et al., 1998) is an artificial neural network architecture specifically designed to capture spatial information and relationship by mimicking the applications of convolution matrices, also called filters or kernels, in image processing. However, instead of using a set of human-defined filters, a CNN is able to learn optimal filters from the dataset on the fly. CNN is mostly used to analyze image data because neighboring pixels are highly correlated and visual patterns are generally translation invariant. These properties allow the model to apply the same filters throughout the image, thereby reducing the number of parameters in the model. Outputs extracted from these filters constitute a feature vector that contains useful representation for the input image. However, as the feature vector from convolution can be large, pooling by taking the maximum or average value is necessary for reducing the vector size.

2.4 Recurrent Neural Network

Recurrent neural network (RNN) is an artificial neural network architecture specifically designed to handle temporal correlations in time series tasks (Elman, 1990). RNN consists of recurrent hidden states which allow it to memorize and utilize knowledge from the past. RNN retains past information by autoregressively integrate the output of previous state with new input during training. However, traditional RNNs still struggle to learn dependencies from distant past in long sequences. To date, several solutions for this limitation have been proposed, including Long Short Term Memory (LSTM) and Gated Recurrent Unit (GRU).

2.5 Long Short Term Memory

Long Short Term Memory (LSTM) was first proposed by Hochreiter and Schmidhuber (Hochreiter and Schmidhuber, 1997). An LSTM has a chain structure like an RNN. However, LSTM has a cell for storing information and gate mechanisms to control the cell state. An LSTM unit consists of three gates: forget gate, input gate and output gate.

2.5.1 Forget gate

The forget gate is useful for deciding how much information to retain inside the cell state. The decision is made through a *sigmoid* layer (Eq. 2.6) based on the input data X_t and the previous hidden state h_{t-1} . The output from this *sigmoid* layer is interpreted as the fraction of previous state to remember, with 0 denotes forgetting and 1 denotes remembering, and is element-wise multiplied to the previous cell state C_{t-1} .

$$f_t = \sigma(W_f * [X_t, h_{t-1}] + b_f) \quad (2.6)$$

2.5.2 Input gate

The input gate decides when to update the cell state and what the new cell state would be. The input gate consists of a *sigmoid* layer and a *tanh* layer. The first layer decides which values will be updated (Eq. 2.7) whereas the second layer generates the new candidate cell state \tilde{C}_t (Eq. 2.8). Both layers receive the input data X_t and the previous hidden state h_{t-1} .

$$i_t = \sigma(W_i * [X_t, h_{t-1}] + b_i) \quad (2.7)$$

$$\tilde{C}_t = \tanh(W * [X_t, h_{t-1}] + b) \quad (2.8)$$

Then, the outputs from the two layers are element-wise multiplied to create a candidate update vector for the cell state. The sum of this candidate cell state and the product of the previous cell state, C_{t-1} , and the *sigmoid* output from the forget gate is set as the new cell state, as shown in Eq. 2.9.

$$C_t = f_t * C_{t-1} + i_t * \tilde{C}_t \quad (2.9)$$

2.5.3 Output gate

The output gate decides how much of the cell state C_t would be transmitted as the output. First, the input data X_t and the previous hidden state h_{t-1} is passed through a *sigmoid* layer to produce the weight vector o_t (Eq. 2.10). Then, this weight vector is multiplied to the *tanh* activation of the cell state C_t to generate the output (Eq. 2.11).

$$o_t = \sigma(W_o * [X_t, h_{t-1}] + b_o) \quad (2.10)$$

$$h_t = o_t * \tanh(C_t) \quad (2.11)$$

These gate mechanisms help mitigate the problem faced by traditional RNNs because they allow the model to learn to discard unimportant information and retain useful information.

2.6 Gated Recurrent Unit

Gated recurrent unit (GRU) is a more recent RNN architecture (Cho et al., 2014). GRU uses gate mechanisms like those of LSTM but slightly differs in the design. There are two gates in GRU: reset gate and update gate.

2.6.1 Reset gate

This gate works like the forget gate in LSTM. The reset gate decides how much information to retain from previous hidden state h_{t-1} via a *sigmoid* layer (Eq. 2.12).

$$r_t = \sigma(W_r * [X_t, h_{t-1}] + b_r) \quad (2.12)$$

2.6.2 Update gate

The update gate decides which past information will be passed to the next state. First, the previous hidden state h_{t-1} and input data X_t are subjected to another *sigmoid* layer (Eq. 2.13).

$$z_t = \sigma(W_z * [X_t, h_{t-1}] + b_z) \quad (2.13)$$

To generate the new candidate state, GRU performs an element-wise multiplication between r_t and h_{t-1} and passes the result to a *tanh* layer (Eq. 2.14).

$$\tilde{h}_t = \tanh(W * [X_t, r_t * h_{t-1}] + b) \quad (2.14)$$

Finally, the new candidate state \tilde{h}_t and the previous hidden state h_{t-1} are weighted averaged according to the weights $1 - z_t$ and z_t produced by the update gate, as shown in Eq. 2.15, to derive the new hidden state.

$$h_t = z_t * h_{t-1} + (1 - z_t) * \tilde{h}_t \quad (2.15)$$

2.7 Encoder-Decoder Sequence to Sequence (Seq2Seq) model

Encoder-decoder model (Figure 2.2) has been used in various fields such as image captioning (Vinyals et al., 2014) and machine translation. Sutskever *et al.* (Sutskever

et al., 2014) presented an encoder-decoder model, also called Seq2Seq, for sequence-to-sequence learning in machine translation tasks. Both the encoder and decoder consist of multilayered LSTMs. As the name implies, LSTM in the encoder is used for encoding information from the input sequence and passing the last hidden state vector to the decoder as its initial state. Then, LSTM in the decoder begins to generate the output sequence. While training the Seq2Seq model, Sutskever et al. (Sutskever et al., 2014) fed the input sequence to the encoder in the reverse order. For example, instead of training the model to map a, b, c to A, B, C , the model has to map c, b, a to A, B, C . This technique improves the training of LSTMs because the input information from a is now close to the corresponding output A , thus helping stochastic gradient descent (SGD) create a tighter connection between the input and the output.

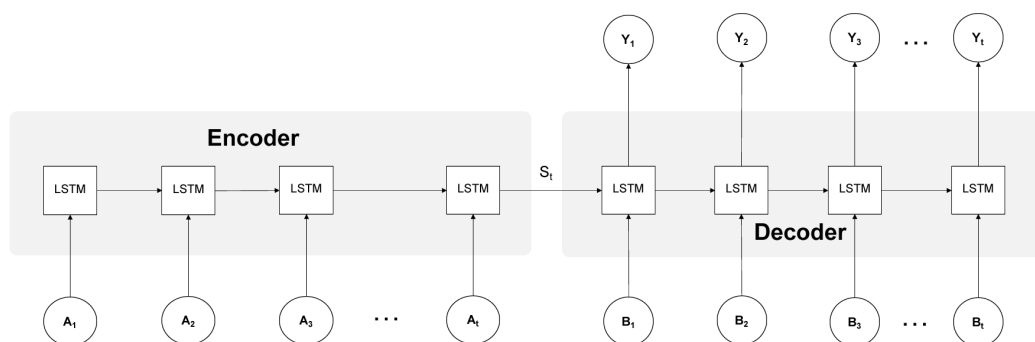


Figure 2.2: **Encoder-Decoder sequence-to-sequence (Seq2Seq) model architecture** Seq2Seq model consists of an encoder and a decoder. The role of the encoder is to embed information from the input A_1, A_2, A_3 and use it as the initial weight for the decoder. The role of the decoder is to generate the output sequence Y_1, Y_2, Y_3 given the initial weight and another input sequence B_1, B_2, B_3 .

Chapter III

RELATED WORKS

UV forecasting has been actively researched because of its usefulness in atmospheric study, heliotherapy, and solar energy production. Most methods rely on similar sets of weather data, including UV, cloud coverage, aerosol, and ozone. The key difference between these methods lie in the computational technique used, which can be categorized into three groups: modeling based on the physics of UV radiation, a hybrid between physics-based modeling and empirical techniques, and deep learning. In this chapter, we explore representative works from these three groups and compare the advantages of each approach.

3.1 Modeling based on the physics of UV radiation

These works use physics knowledge to calculate the theoretical amount of UV radiation that travels from the Sun to Earth. The theoretical amount of UV that reaches the Earth's outer atmosphere is called extraterrestrial UV. The theoretical amount of UV that gets through the ozone layer is called clear-sky UV. Factors included in these calculations are the Earth-Sun distance, solar zenith angle, and the thickness of ozone layer (Krzyściński et al., 2015; Allaart et al., 2006; Leccese et al., 2018).

However, the amount of UV radiation that actually reaches the Earth's surface may be heavily reduced by the Earth's atmosphere and pollution. To account for this discrepancy, some works proposed the Cloud Modification Factor (Krzyściński et al., 2015; Sudhivabha et al., 2006) which approximates the reduction in UV radiation due to the cloud coverage. The final predicted UV in this case would be the product between the theoretical clear-sky UV and the Cloud Modification Factor. One work by Zavodka and Reichrt (Zavodska and Reichrt, 1985) bypassed the need to estimate modification factor by directly learning a formula for calculating UV radiation from solar total irradiance. Their equation is a simple linear model 3.1 fitted to the observed UV and solar total

irradiance in Bratislava, Slovakia.

$$I_{UV} = 0.054 * I + 0.052 \quad (3.1)$$

An advantage of physics-based modeling is that the resulting daily UV prediction naturally follows a perfect bell-shaped pattern, allowing this approach to perform well on Sunny days even in regions that do not collect any UV data. Nonetheless, as this approach does not take the seasonal weather effect into account, it will produce systematic errors depending on the season.

3.2 Hybrid between physics-based modeling and empirical techniques

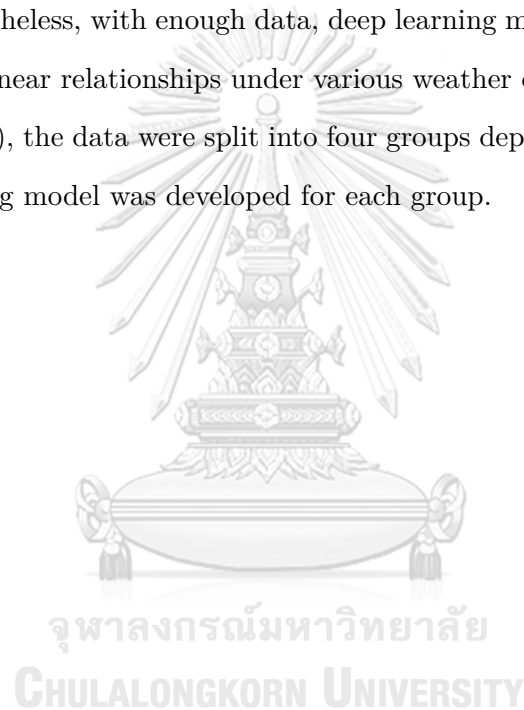
The main difference between a hybrid method and a physics-based modeling is how model coefficients are determined. While physics-based modeling derives coefficient values using theoretical knowledge and physical constants, the hybrid method uses regression technique to estimate the coefficients from past observations (Sudhibrabha et al., 2006; Deo et al., 2017; Feister et al., 2011; Foyo-Moreno et al., 1999; Allaart et al., 2006). This lets the hybrid model learn seasonal weather effects and be more accurate in regions that have collected sufficient data. However, regression techniques can be susceptible to noises and may overfit the observed data distribution.

In Thailand, Sudhibrabha (Sudhibrabha et al., 2006) uses two linear regression models for UV forecasting. The first model forecasts the amount of ozone. The second model incorporates the predicted ozone and other physical features, such as the Earth-Sun distance and the solar zenith angle, to forecast the amount of UV. Finally, the predicted UV is multiplied to a Cloud Modification Factor that is derived from weather forecast.

3.3 Deep learning

Recent works in the energy domain have successfully utilized recurrent neural network (RNN) (Elman, 1990) architectures, such as Long Short-Term Memory (LSTM)

(Hochreiter and Schmidhuber, 1997) and Gated Recurrent Unit (GRU)(Cho et al., 2014), to predict solar photovoltaic power production(Qing and Niu, 2018; Wang et al., 2018; Husein and Chung, 2019; Gensler et al., 2016; Huang et al., 2019). Unlike the aforementioned approaches, deep learning model relies solely on past observations of UV or other UV-related features (Qing and Niu, 2018; Wang et al., 2018; Elminir et al., 2008; Jacovides et al., 2015). Although deep learning can yield an effective forecasting model(Siami-Namini and Namin, 2018), it suffers from overfitting to the training data and struggles to perform well in different geographical regions like other regression approaches. Nonetheless, with enough data, deep learning model can be trained to handle complex non-linear relationships under various weather conditions. In Wang's work (Wang et al., 2018), the data were split into four groups depending on the weather type and a deep learning model was developed for each group.



Chapter IV

METHOD

This chapter explains the datasets, data preprocessing, and our proposed model architecture. This chapter was taken from our manuscript which has been published (Raksasat et al., 2021).

4.1 Surface UV and weather data acquisition

Surface UV radiation, total ozone column, cloud coverage, and aerosol optical depth at 500nm (AOD500), were collected at the Faculty of Science, Silpakorn University, Nakhon Pathom, Thailand (13.82°N, 100.04°E) from January 2009 to May 2019. UV intensity was measured every 10 minutes from 5 AM to 7 PM at 1-nm wavelength interval from 280 nm to 400 nm in mW/m² unit using a DMc150 double monochromator (Bentham Instruments, Berkshire, UK). Ozone, cloud coverage, and AOD500 data were collected from 6 AM to 6 PM from January 2011 to December 2018. Total ozone column data were measured daily in Dobson unit (DU) via an OMI/Aura satellite (NASA, Washington, DC, USA). Hourly AOD500 data were measured by a ground-based CE318 sunphotometre (Cimel Electronique, Paris, France) and calibrated by the Aerosol Robotic Network (NASA, Washington, DC, USA). Cloud coverage data were estimated on a 0-10 scale from recorded images of the sky every hour through a PSV-100 Skyview instrument (Prede Company, Tokyo, Japan). The distributions of UV radiation, cloud, ozone, and AOD500 in Nakhon Pathom throughout the year are shown in Figure 4.1 a-d, respectively.

Hourly downward surface UV radiation in J/m², total ozone column in kg/m², and mid cloud coverage were also downloaded from ERA5(Hersbach et al., 2018) for London, England (51.5°N, 0°E) and Tokyo, Japan (35.75°N, 139.75°E) from 5 AM to 7 PM from January 2011 to December 2019. It should be noted that ERA5 datasets were generated from a combination of actual observation (every 3-hour) and computational

reanalysis. ERA5 downward UV radiation data cover the 200–440 nm wavelength range.

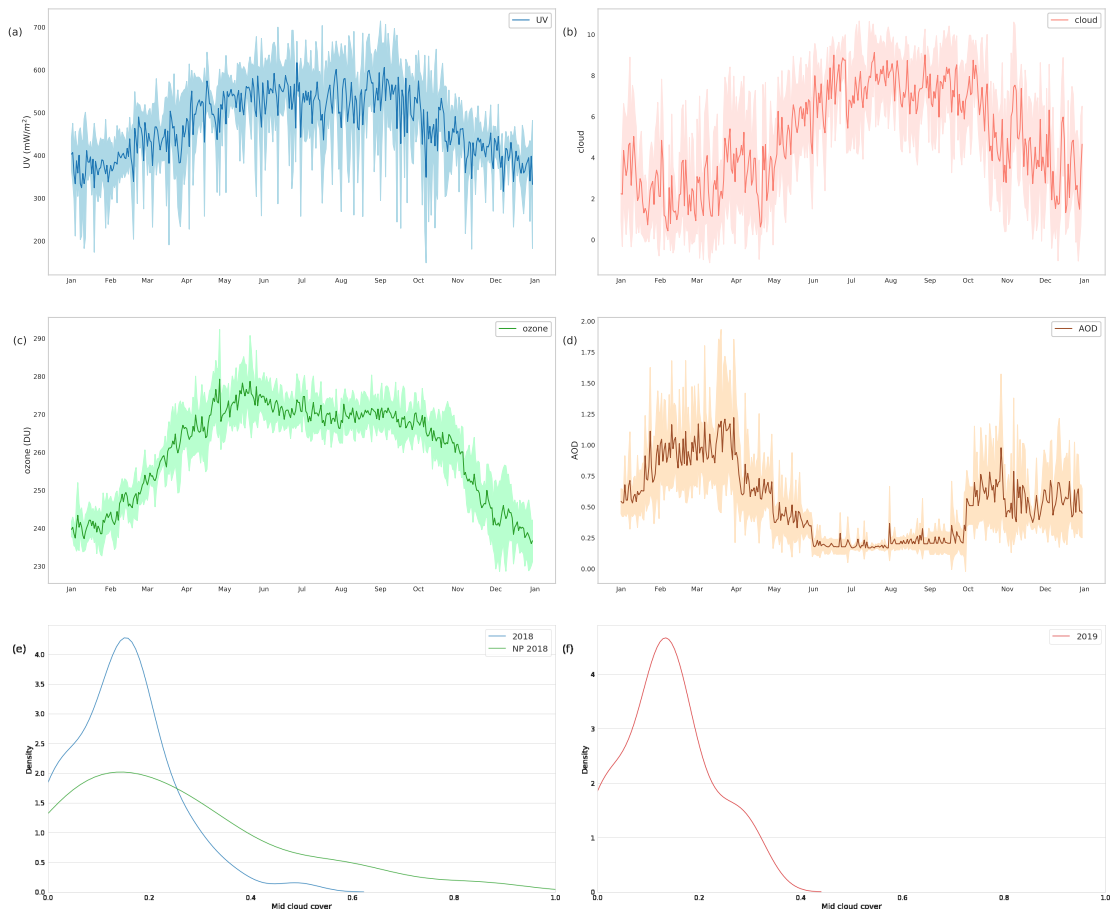


Figure 4.1: Characteristics of UV and weather conditions at Nakhon Pathom, Thailand. Daily maximums are shown for UV irradiance, total ozone column, and AOD500. Daily averages are shown for cloud coverage. Dark lines indicate the average across 2009–2017. Shaded areas indicate the ± 1 standard deviation range. (a) Annual surface UV irradiance. (b) Annual cloud coverage. (c) Annual total ozone column. (d) Annual AOD500. (e) The distribution of cloud coverage in the validation set (UV data from the year 2018). Both Silpakorn University’s observations and ERA5 data were shown. (f) The distribution of cloud coverage in test set (UV data from the year 2019). Information from Silpakorn University is unavailable.

4.2 Data cleaning and preprocessing

Surface UV radiation exhibits an annual seasonal pattern. We used this pattern as a justification for using UV data of the same dates from adjacent years to impute each missing data point. This is crucial because missing UV data often arise from sensor malfunction which typically spans multiple days. Also, because the artificial neural network model cannot handle missing values, imputation increases the number

of data points that can be used to train and test the model. Specifically, we impute each missing data point with the average UV radiation from adjacent 10-minute time steps, the same time steps from adjacent days, and the same dates from adjacent years. The ranges of adjacent time steps, days, and years that were used for imputation are 2, 5, and 2, respectively. Imputed data were visually inspected to ensure that the overall UV intensity follows the expected bell-shaped pattern with a peak at around noon. In Thailand, this bell-shaped pattern is often observed from October to January where there are few rainy and cloudy days. The Nakhon Pathom UV data from 2014 were excluded from further considerations as there is a technical problem with the instrument.

Nakhon Pathom UV data were split into a training set (2009-2017), for optimizing the parameters of artificial neural network models, a validation set (2018), for determining when to stop the optimization process, and a test set (2019), for evaluating the performance of the final models. We found that using the whole training set, i.e., using UV data from all dates and times, to train the models yielded the best performance. For the validation and test sets, we further exclude data from days with anomalous UV intensity profiles to prevent them from influencing the evaluation of the models. Specifically, we removed data from days whose UV profiles are highly skewed (absolute skewness greater than 0.3), disproportional (ratio between maximal and minimal irradiances greater than 15), or out of expected range (maximal irradiance above 400 or below 150 mW/m²). The distributions of cloud coverage in the validation and test datasets are shown in Figure 1e and 1f, respectively. Finally, the antipsoriatic irradiance at each time point was calculated from 280-400 nm UV data based on published psoriasis clearance action spectrum formula (Krzyścin et al., 2012; Parrish and Jaenicke, 1981; Fischer et al., 1984).

For evaluating the impact of incorporating ozone and AOD₅₀₀ information as input into SurfUVNet, because these data were available only up to 2018, we re-split the dataset by setting data from 2009-2016 as the training set, data from 2017 as the validation set, and data from 2018 as the test set. The same quality filter for excluding data from days with poor UV profiles defined above was also applied to these validation

and test sets. SurfUVNet model variants with and without ozone and AOD500 as input were then trained and evaluated together on this data split. We also test the relationship between ozone and AOD500 to UV. With training SurfUVNet to predict ozone and AOD500 by receives UV as inputs.

4.3 SurfUVNet model architecture

Encoder-decoder-based model is a kind of deep learning model that has been successfully applied to various applications such as image captioning(Vinyals et al., 2014) and machine translation(Sutskever et al., 2014). In the context of UV forecasting, an encoder-decoder model can be used to translate a sequence of past observed UV radiations into a sequence of future UV radiations. The model consists of two parts: encoder and decoder as shown in Figure 4.2. Both parts consist of multilayered LSTMs. As the names implied, the LSTMs in the encoder is used for encoding information from the input sequence while the LSTMs in the decoder decoded that information to generate the output sequence.

As the input to our model, we use a sequence of antipsoriatic data from the previous day, denoted as $[A_1, A_2, \dots, A_t]$ and a sequence of antipsoriatic data from the previous year, denoted as $[B_1, B_2, \dots, B_t]$. For the model variant which also accepts AOD500 and ozone, the inputs A_i 's and B_i 's will include these data of the same time-of-day from previous days and previous year as well. To handle differences in data resolution for various features (10-minute for UV irradiance, hourly for AOD500, and daily for ozone), the values of features with lower resolutions were duplicated to match the highest resolution.

Since the antipsoriatic values are seasonal in nature, we also include day-of-year information as the input by encoding the day-of-year on a circular index defined as:

$$\text{CircularIndex}_{\text{Date}} = \left[\sin 2\pi \left(\frac{\text{day}}{365} \right), \cos 2\pi \left(\frac{\text{day}}{365} \right) \right] \quad (4.1)$$

The circular date feature helps the model to learn the seasonal pattern. The model predicts future antipsoriatic values, $[\bar{y}_1, \bar{y}_2, \dots, \bar{y}_t]$.

4.3.1 Encoder

The encoder takes the previous day sequence $[A_1, A_2, \dots, A_t]$ and the circular date feature as input. We use a bi-directional (Schuster and Paliwal, 1997) LSTM as the first layer to help the model learn the temporal effect in both directions. The latter layers are uni-directional LSTM that will capture the information and pass the information to the decoder via the final cell state, S_t .

4.3.2 Decoder

The decoder takes $[B_1, B_2, \dots, B_t]$ as input and uses it to future predict antipsoriatic values. The first layer of the decoder is an LSTM layer that uses S_t from the decoder as the initial value of the cell state. We also add two fully connected layers with sigmoid activation function with the dropout (Srivastava et al., 2014) rate of 0.2 after the LSTM layer for the final output.

Before feeding the input data to the model, we denoised the input antipsoriatic data with the Savitzky–Golay filter (Savitzky and Golay, 1964). Applying the filter, smooth out the input data, removing any possible noise spikes in the data. However, we do not apply this processing to the target output data. If we train the model to predict the denoised data, the model is learning to predict the unrealistic data and will not be able to handle noises in the UV intensities. Then, we normalized the antipsoriatic data into a range of $[0,1]$. We trained the model using quantile loss (Koenker and Hallock, 2001) defined as:

$$L_{\text{QUANTILE}} = \frac{1}{N} \sum_{i=1}^N \max(q(\bar{y}_i - y_i), (q-1)(\bar{y}_i - y_i)) \quad (4.2)$$

where y_i is the actual value and \bar{y}_i is the predicted value, q is a quantile value that balances the penalties of overestimates and underestimates. If q is more than 0.5,

the quantile loss gives more penalty to overestimated predictions and vice versa. In our work, we set q to 0.33 to favor overestimation rather than underestimation because underestimated results can cause sunburn to patients due to a prescribed sunbathing time that is too long.

4.4 Model training

We used Adaptive Moment Estimation (ADAM)(Kingma and Ba, 2014) as the optimizer. The learning rate was initially set to 0.0005 and iteratively reduced linearly by $1e-7$ per epoch. Models were trained for 2,000 epochs with a batch size of 256. We measure the model performance with mean absolute percentage error metric (MAPE) as shown in Eq. 4.3.

$$MAPE = \frac{1}{N} \sum_{i=1}^N \left| \frac{\bar{y}_i - y_i}{y_i} \right| \quad (4.3)$$

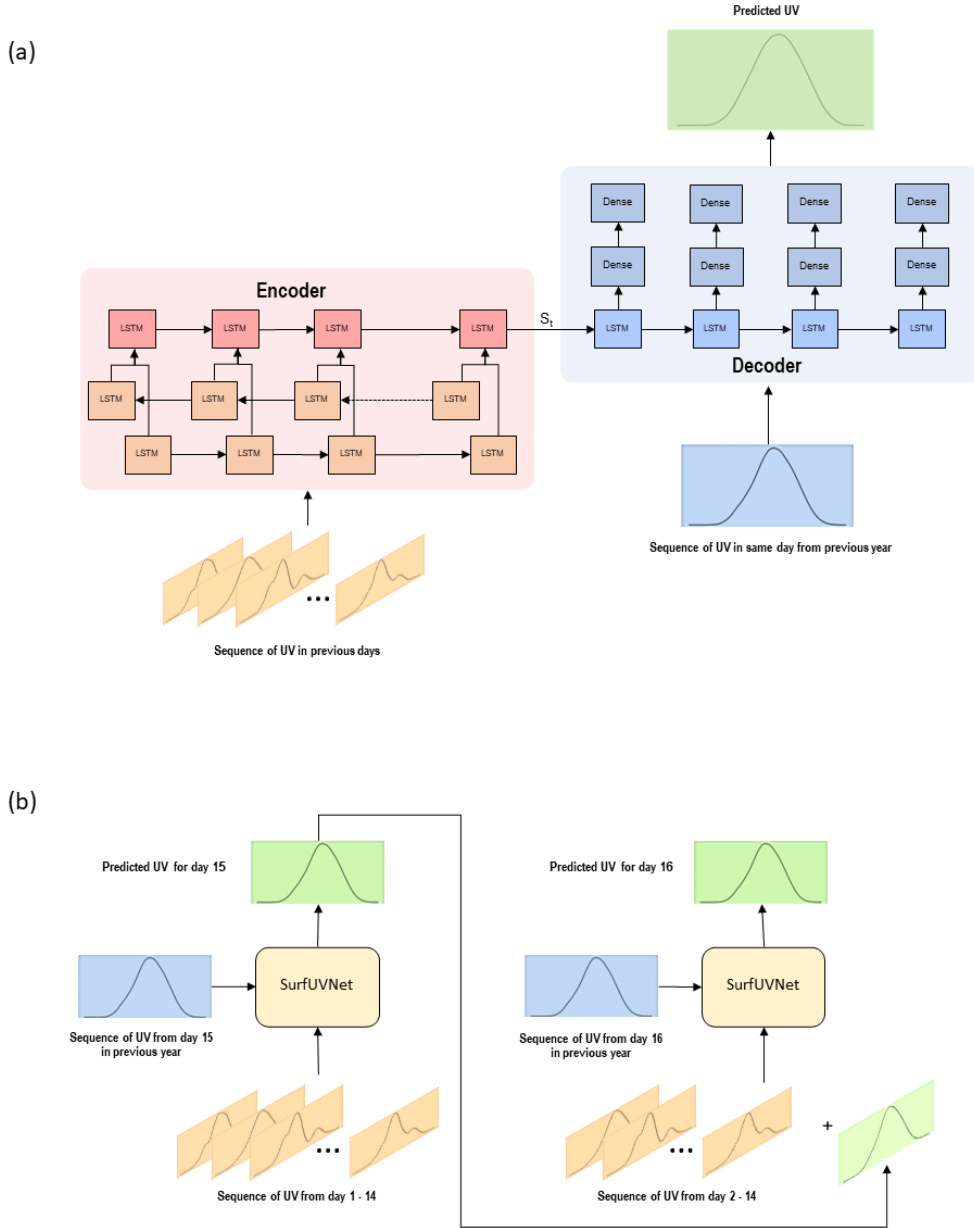


Figure 4.2: **Schematic of SurfUVNet.** (a) The underlying encoder-decoder neural network architecture showing the flow of data from the encoder to the decoder via the central connection denoted by S_t . LSTM and Dense indicate the Long Short-Term Memory and fully connected neural network layers, respectively. UV data from days prior to the forecast date are fed into the encoder part while UV data from the same date of the previous year are fed into the decoder part. The model forecasts next-day UV radiation at 10-minute resolution. (b) The auto-recursive mode for long-term UV forecasting. To forecast UV radiation for the next N days, SurfUVNet first forecasts next-day's UV radiation profile and then uses the prediction as input to forecast UV radiation profile for the day after. This process is repeated until the forecasts for the next N days are generated.

Chapter V

RESULT

In this chapter, we present the results from the experiments with datasets described in previous chapter. We tested our model with different input range to find the input that give us a best result and use different input to find the impact on model performance. we also tested and compared our model when using in next-day and long-term prediction with other benchmark models. This chapter was taken from our manuscript which has been published (Raksasat et al., 2021).

5.1 SurfUVNet model architecture

The task of forecasting in general can be formulated as a problem of finding the best approximation for the relationship between past and future observations. For surface UV radiation, which exhibits an annual seasonal pattern, the profile of next-day UV radiation can be modeled using not only data from previous days but also data from previous years. Here, we adapted an encoder-decoder architecture, which can effectively capture relationship between sequence data, to develop an artificial neural network model for forecasting next-day surface UV radiation. Our model, named SurfUVNet, takes in UV radiation profiles of the past 7, 14, or 21 days through the encoder and passes the encoded information to the decoder. The decoder then takes in the UV radiation profile of the same date as the next day but from last year, combines it with information from the encoder, and then generates the next-day forecast (Figure 4.2 a). Intuitively, because UV radiation exhibits annual seasonal pattern, our approach models the next-day UV radiation profile as a transformed version of last year's data and uses recently observed UV pattern to learn the appropriate transformation.

Finally, to forecast UV radiation profile further into the future, our approach essentially performs next-day forecast repeatedly via an auto-regressive approach. For example, if we define today as the day N , to predict the UV radiation profile for next week, or day $N + 7$, our model first uses data from days $N-6$, $N-5$, ..., N to forecast UV for the day $N + 1$, and then uses the data from days $N-5$, $N-4$, ..., N , and the forecast for the day $N + 1$ to forecast UV for the day $N + 2$, and so on (Figure 4.2 b).

5.2 Benchmark procedure

We evaluated the performance of SurfUVNet (also called Seq2Seq-14 here) against four alternative models: a simple model that uses the previous day UV radiation pattern as the prediction, an empirical approach that combined physics knowledge to define the interactions between UV-related factors with regression technique to learn coefficient values, which is currently in used by the Thai Meteorological Department (Sudhibrabha et al., 2006), a CNN-LSTM neural network model developed for solar power forecasting (Wang et al., 2018), and an implementation of bidirectional GRU neural network model which is often used in time series forecasting applications. As prior study has shown that the CNN-LSTM model benefits from additional smoothing of UV data from rainy days (Wang et al., 2018), we considered two CNN-LSTM model implementations: one without smoothing and one with Savitzky–Golay filter (Savitzky and Golay, 1964) (denoted by CNN-LSTM and CNN-LSTM-SG in Figure 5.1 a and Table 5.1). To fairly compare model performance, the validation and test datasets were subjected to quality filtering to remove days with highly skewed and out-of-range UV irradiance values (see Methods) where all models are expected to perform poorly on. However, it should be noted that this does not mean that our validation and test sets consist of only clear-sky data. The distribution of cloud coverage shows that both datasets contain many days with cloud coverage above 0.2 and up to 0.4 or more (Figure 4.1 e and 4.1 f).

5.3 Next-day antipsoriatic irradiance forecast for Nakhon Pathom dataset

All artificial neural network models were trained using the same UV data from 2011 to 2017 and evaluated on the same UV data from 2018 and 2019 while the regression model based on Earth-Sun distance and total ozone column was fit to UV and ozone data of the same year. All models were trained to forecast next-day antipsoriatic irradiance at 10-minutes resolution. Furthermore, as past UV radiation profile is a critical input data for artificial neural network models, we tried inputting data from 7, 14, or 21 days prior to the forecast date to explore whether the models benefit from seeing data from more distant past.

Overall, SurfUVNet achieves the best next-day forecasting performance with mean absolute percentage errors (MAPE) of 10.41 and 10.51 on the validation and test sets, respectively (Seq2Seq models in Figure 5.1 a and Table 5.1). It should be noted that while the CNN-LSTM-SG model can also reach similar levels of performance (MAPE of 11.39 and 11.84), it is highly sensitive to the length of input UV data. Changing the length of input UV data from 7 days to 14 or 21 days significantly raises the MAPE of CNN-LSTM-SG models to 13.87-17.74. In contrast, the performance of SurfUVNet is stable with respect to the length of the input. Furthermore, SurfUVNet achieves consistent forecasting accuracy throughout the day while the CNN-LSTM-SG model produce significantly higher forecast error during the morning and afternoon hours (8AM-9AM and 2PM-4PM) compared to the middle of the day (Figure 5.1 b and 5.1 c). Lastly, comparison of ground truth antipsoriatic irradiance and SurfUVNet's forecast confirmed that SurfUVNet's prediction closely mimics the expected bell-shaped pattern of daily UV radiation in both validation and test sets (Figure 5.1 d and 5.1 e).

5.4 Next-day downward solar UV irradiance forecast for Tokyo and London datasets

All models were further evaluated on hourly downward solar UV irradiance data obtained from ERA5 for Tokyo, Japan and London, England, which represent different weather regimes from Thailand's. In contrast to the seasonal cloud coverage pattern at

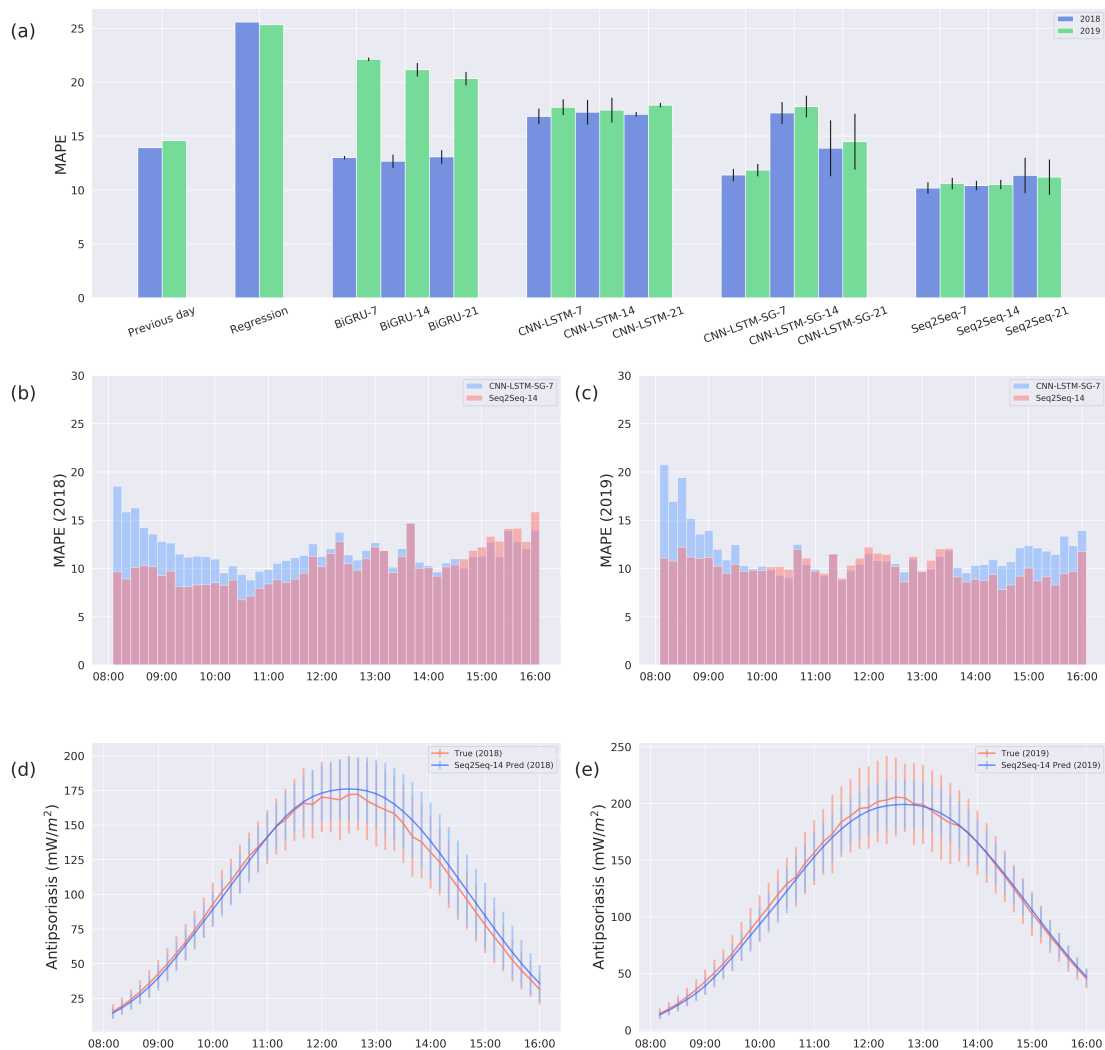


Figure 5.1: Results on Nakhon Pathom dataset were shown. (a) Comparison of the mean absolute percentage errors (MAPE) for the next-day antipsoriatic irradiance forecast between SurfUVNet (Seq2Seq-14) and four benchmark models (see Methods). Previous day model simply predicts next-day's UV radiation to be the same as today's. Regression model refers to the regression model based on Earth-Sun distance and total ozone column currently in used by the Thai Meteorological Department (Sudhibrabha et al., 2006). BiGRU is an artificial neural network architecture that is often utilized for time series forecasting. CNN-LSTM, and CNN-LSTM-SG are artificial neural network models that were recently applied to UV forecasting in the energy domain (Wang et al., 2018). The tags -7, -14, and -21 designate the length of UV data, in days prior to the forecast date, that were input into each model. (b) Distribution of MAPE for the validation set (UV data from 2018) throughout the times of the day. Results for the best performing models, namely CNN-LSTM-SG-7 and SurfUVNet (Seq2Seq-14), are shown. (c) A similar plot showing distribution of MAPE for the test set (UV data from 2019). (d) Comparison of ground truth UV data and forecasts made by SurfUVNet for the validation set (UV data from 2018). Error bars indicate one-standard deviation ranges. (e) A similar plot for the test set (UV data from 2019)

Nakhon Pathom (Figure 1b), cloud coverage for Tokyo and London fluctuates around 0.2-0.4 year-round (Figure 5.2). Furthermore, day-to-day variation in UV radiation profiles are much higher in Tokyo and London compared to Nakhon Pathom, as indicated by much higher MAPE between today’s and the next day’s UV profiles (Table 5.1 and Table 5.2, 21.78-35.50 for Tokyo, 18.14-43.57 for London, and 13.93-14.58 for Nakhon Pathom). Overall, SurfUVNet performs competitively, achieving MAPE of 12.72 and 17.74 for the next-day forecast for Tokyo and London datasets, respectively (Table 5.2). The regression model based on Earth-Sun distance and total ozone column performs much better on these datasets than on Nakhon Pathom’s (Table 5.1 and Table 5.2, MAPE of 16.52-19.17 on ERA5 compared to 25.52-25.57 on Nakhon Pathom) and only slightly worse than the artificial neural network approaches. Again, it should be noted that the validation and test sets contain many days with considerable cloud coverage (Figure 5.3).

Model	Validation MAPE (2018, 8AM-4PM)	Test MAPE (2019, 8AM-4PM)
Previous day model	13.93	14.58
Regression model based on Earth-Sun distance and total ozone column (Sudhibrabha et al., 2006)	25.57	25.32
BiGRU-7	13.00 ± 0.16^b	22.12 ± 0.33
BiGRU-14	12.66 ± 0.62	21.15 ± 1.20
BiGRU-21	13.07 ± 0.63	20.33 ± 0.47
CNN-LSTM-7 (Wang et al. (2018))	16.82 ± 0.73	17.67 ± 0.91
CNN-LSTM-14 (Wang et al. (2018))	17.21 ± 1.15	17.40 ± 0.44
CNN-LSTM-21 (Wang et al. (2018))	17.02 ± 0.20	17.87 ± 0.24
CNN-LSTM-SG-7	11.39 ± 0.57	11.84 ± 0.63
CNN-LSTM-SG-14	17.14 ± 1.01	17.74 ± 0.70
CNN-LSTM-SG-21	13.87 ± 2.59	14.48 ± 1.96
Seq2Seq-7	10.18 ± 0.53	10.60 ± 0.34
Seq2Seq-14 (SurfUVNet)	10.41 ± 0.43	10.51 ± 0.41
Seq2Seq-21	11.35 ± 1.64	11.19 ± 0.33

Table 5.1: Mean absolute percentage errors (MAPE) of the next-day antipsoriatic irradiance forecasting produced by SurfUVNet and benchmark models.

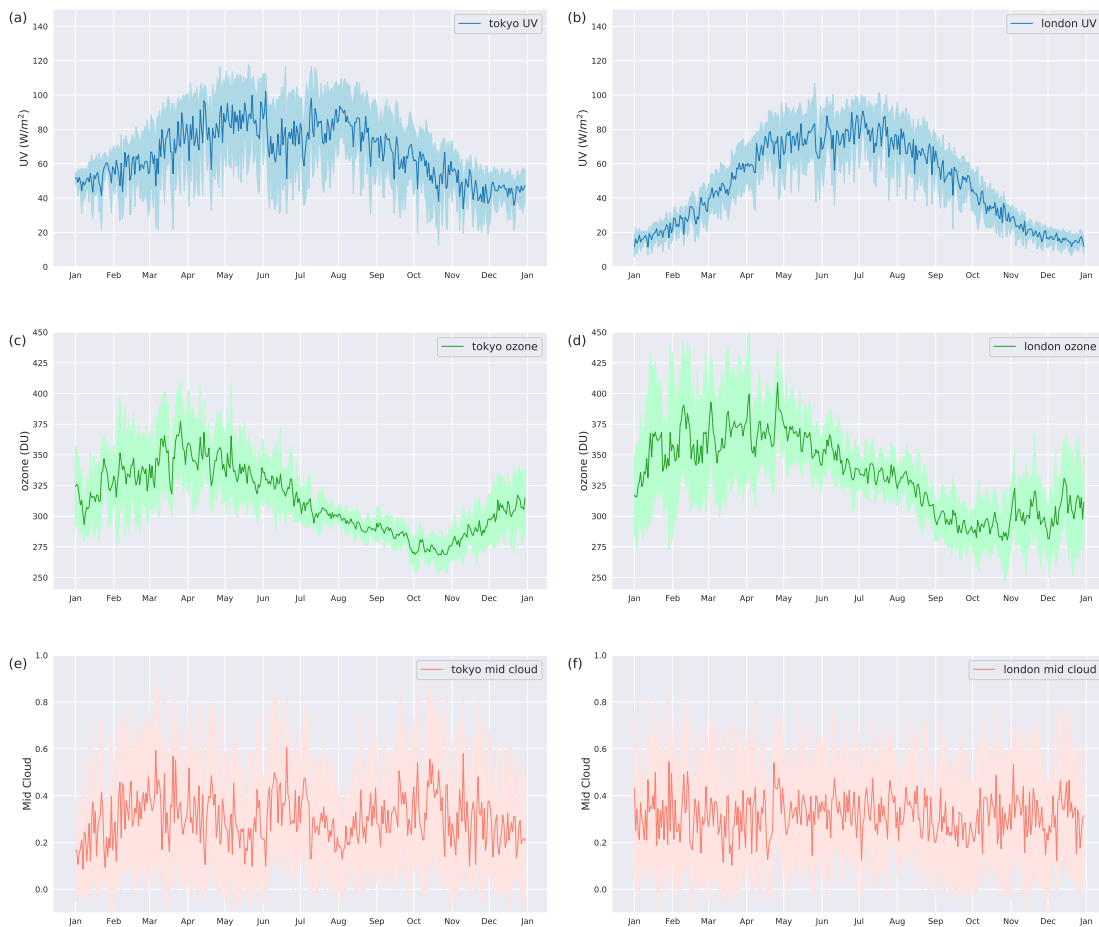


Figure 5.2: **Characteristics of UV and weather conditions at Tokyo, Japan and London, England.** Daily maximums from ERA5 datasets are shown. Dark lines indicate the average across 2009-2017. Shaded areas indicate the ± 1 standard deviation range. (a) Annual downward surface UV irradiance at Tokyo. (b) Annual downward surface UV irradiance at London. (c) Annual total ozone column at Tokyo. (d) Annual total ozone column at London. (e) Annual cloud coverage at Tokyo. (f) Annual cloud coverage at London.

5.5 Adding weather information does not improve forecasting

As atmospheric conditions can reflect and scatter UV radiation before it reaches the Earth's surface, we tried incorporating total ozone column, atmospheric aerosol (AOD500), and cloud coverage data into SurfUVNet. However, cloud coverage data contain many missing values that could not be imputed due to the irregularity of the data and had to be excluded from model development. Instead, we used cloud coverage data to evaluate whether SurfUVNet overestimates the amount of UV radiation when the weather is cloudy. This reveals that SurfUVNet's forecasting errors weakly correlate

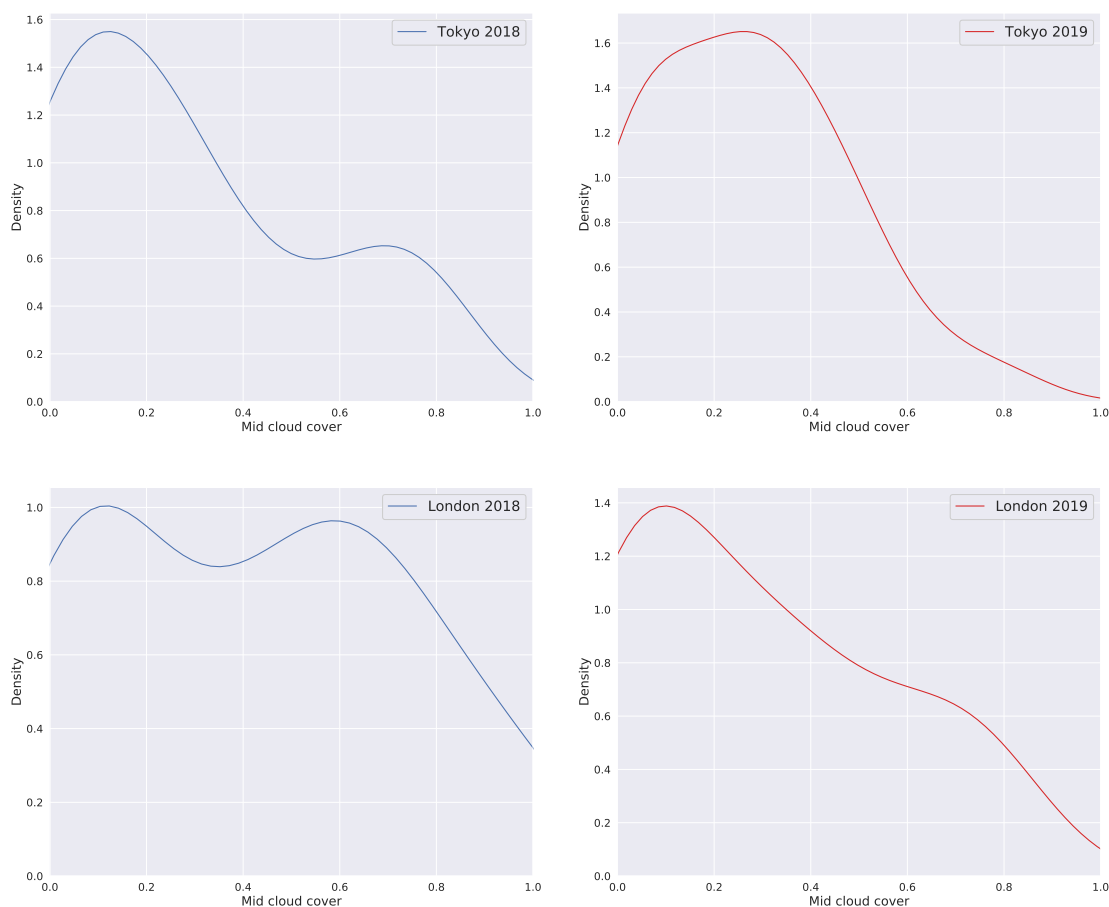


Figure 5.3: **The distribution of cloud coverage in ERA5 validation and test sets.** Mid cloud coverage data are shown. (a) Cloud coverage distribution for validation set (UV data from year 2018) for Tokyo. (b) Test sets (UV data from year 2019) for Tokyo. (c) Validation set (UV data from year 2018) for London. (d) Test sets (UV data from year 2019) for London.

Model	Tokyo		London	
	Validation MAPE (2018, 8AM-4PM)	Test MAPE (2019, 8AM-4PM)	Validation MAPE (2018, 8AM-4PM)	Test MAPE (2019, 8AM-4PM)
Previous day model	21.78	35.50	18.14	43.57
Regression model based on Earth-Sun distance and total ozone column (Sudhibrabha et al. (2006))	16.68	16.52	18.68	19.17
CNN-LSTM-SG-7	14.75 ± 0.41	15.77 ± 0.33	13.14 ± 0.35	16.27 ± 0.54
CNN-LSTM-SG-14	13.18 ± 0.28	14.99 ± 0.51	12.19 ± 0.19	17.78 ± 0.19
Seq2Seq-14 (SurfUVNet)	11.83 ± 0.44	12.72 ± 0.67	11.54 ± 0.50	17.74 ± 0.19

Table 5.2: Mean absolute percentage errors (MAPE) of the next-day antipsoriatic irradiance forecasting produced by SurfUVNet and other models on the ERA5 Tokyo and London datasets.

with cloud condition (Figure 5.4 , spearman rank correlation = 0.16776, -0.04546, and 0.20229 for Nakhon Pathom, Tokyo, and London 2019 datasets). For Nakhon Pathom dataset, SurfUVNet’s forecast error stays roughly the same before shifting upward when cloud coverage goes above 0.7 (Figure 5.4 a). For Tokyo dataset, SurfUVNet’s error is not correlated with cloud coverage at all (Figure 5.4 b). SurfUVNet’s error shows the clearest correlation with cloud coverage in London dataset (Figure 5.4 c). Addition of ozone and AOD500 data into SurfUVNet does not improve the performance of the base model that utilizes only UV data (Figure 5.5). The model with ozone and AOD500 data achieves MAPE of 15.33 on the validation set (data from 2017) and MAPE of 13.91 on the test set (data from 2018), while the base model achieves MAPE of 14.32 and 13.60, respectively. This may be because ozone and AOD500 data were collected at lower frequency (hourly versus every ten minutes) and at a shorter time period during the day (6AM-6PM versus 5AM-7PM) than UV data. Although data from the early morning and late evening hours where the amount of UV radiation is almost nonexistence should not contribute much to the forecasting of UV radiation during daylight hours, we found that withholding UV data from 6-8AM and 4-6PM from the model slightly raises error from 10.51 to 11.78 MAPE (Wilcoxon signed rank test result is not significant with p-value = 0.5567). We also trained SurfUVNet to predict ozone and AOD500 using only UV data as input for finding the model ability in mapping the correlation between UV and pollution features. The error of ozone and AOD500 prediction is 3.07 and 57.77 MAPE in validation set and 2.33 and 34.76 MAPE in test set. This result proves that the model can learn the relationship between UV and ozone while terrible at learning the AOD500 and UV relationship. Lastly, to evaluate the impact of uncertainty of next-day ozone and AOD500 on the forecast performance, a variant of SurfUVNet was trained with the actual values of next-day ozone and AOD500. This does not reduce the forecast error (MAPE of 15.70 and 15.50 on the validation and test sets, respectively), indicating that the limitation lies elsewhere.

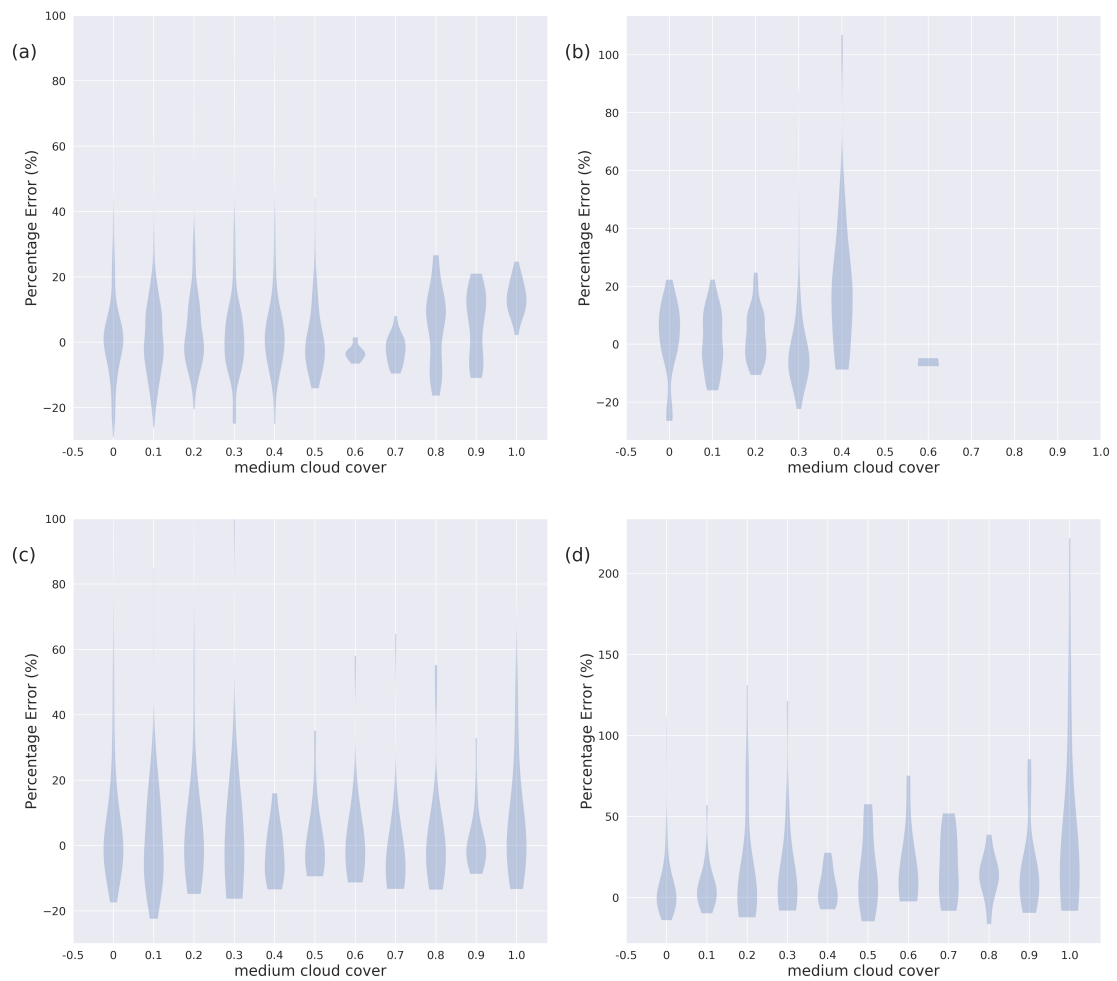


Figure 5.4: **SurfUVNet’s forecast error weakly correlates with cloud coverage.** Violin plots showing the distribution of SurfUVNet’s forecast error in 1-hour interval with various cloud coverage. Errors on the test sets (UV data from year 2019) are shown. (a) Nakhon Pathom dataset. (b) Tokyo dataset. (c) London dataset. (d) Heliotherapy sunbathing sessions planned by photodermatologist at King Chulalongkorn Memorial Hospital. Each data point that constitutes the violin plots correspond to the error between predicted and actual antipsoriatic irradiances that a patient would be exposed to if he or she were to sunbath according to dermatologist’s planning.

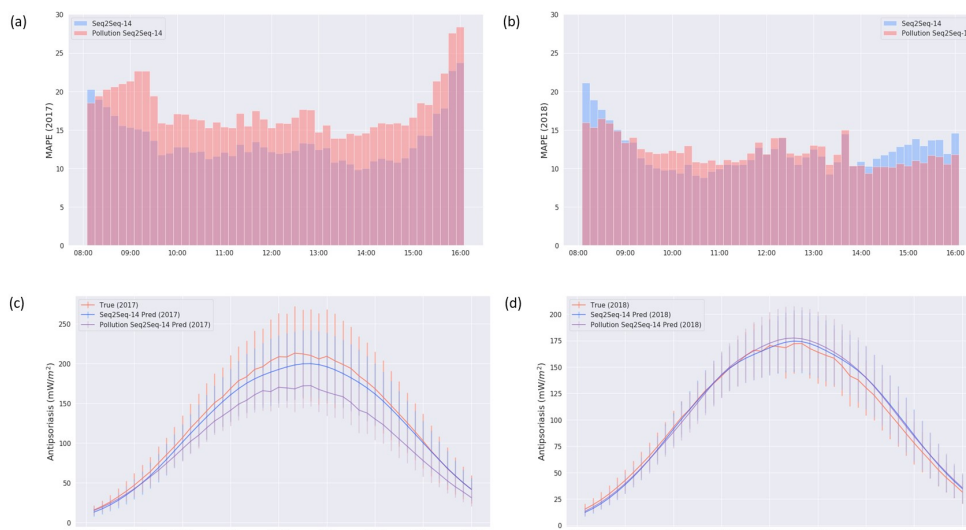


Figure 5.5: **Comparison of SurfUVNet performance with and without ozone and AOD500 as input.** It should be noted that as AOD500 data at Nakhon Pathom for the year 2019 were not available, UV data from year 2017 were set as the validation set and UV data from year 2018 were set as the test set here. (a) Distribution of MAPE for the validation set (UV data from 2017) throughout the times of the day. (b) A similar plot showing distribution of MAPE for the test set (UV data from 2018). (c) Comparison of ground truth UV data and forecasts made by SurfUVNet for the validation set (UV data from 2017). Error bars indicate one-standard deviation ranges. (d) A similar plot for the test set (UV data from 2018).

5.6 Long-term antipsoriatic irradiance forecasting

Long-term UV forecasting is essential for heliotherapy applications as it allows clinicians and patients to plan sun-bathing schedule in advance and make necessary adjustments to the schedule to achieve the desire UV radiation dosage. We explored two approaches for forecasting antipsoriatic irradiance for up to a month into the future (Figure 5.6 a). The first approach is to train a collection of artificial neural network models, each making the forecast for a specific date that is a certain number of days into the future. In other words, we trained one model for making the next-day forecast, one model for making the forecast for the day after that, and so on. The second approach is to train a single model for making the next-day forecast and then autoregressively use the next-day forecast as in input to make the forecast for the day after that. Evaluation on Nakhon Pathom 2018-2019 UV datasets showed that the performance of the autoregressive approach is quite stable with average MAPE of 13.70-15.79 for forecasting up

to 28 days into the future (Table 5.3 and Figure 5.6 b). On the other hand, developing specific models for specific days performs well on the 2019 dataset but poorly on the 2018 dataset (MAPE of 11.46 vs 18.38 for forecasting up to 28 days into the future). We also additionally explored the possibility of training a model that can forecast UV profiles of multiple days at once, but the performances were much worse than the two methods described above (MAPE of 29.49 and 49.69 for forecasting the next 7 days at once on the 2018 and 2019 datasets, respectively). Hence, we decided to choose the autoregressive approach for SurfUVNet. It should be noted that the regression approach based on Earth-Sun distance and ozone information performed poorly on Nakhon Pathom's UV data even for next-day forecast (Table 5.1, MAPE of 25.32-25.57).

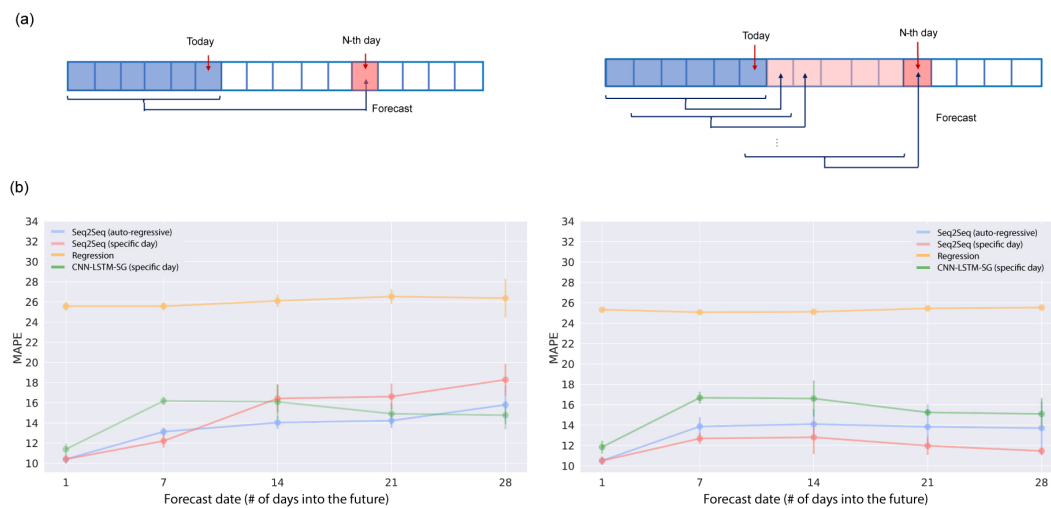


Figure 5.6: **Long-term antipsoriatic irradiance forecasting.** Results on Nakhon Pathom dataset were shown. (a) Diagram of two approaches for making long-term forecast: developing specific artificial neural network model for making forecast for a specific day that is a certain number of days into the future (left) and autoregressively using the next-day forecast as input for making forecast for the day after that (right). (b) Long-term antipsoriatic irradiance forecasting performance for up to 28 days into the future on the validation set (UV data from 2018) and the test set (UV data from 2019). Performance for SurfUVNet, the regression model based on Earth-Sun distance and total ozone column, and the best CNN-LSTM models were shown.

Model	Target Day	Validation MAPE (2018, 8AM-4PM)	Test MAPE (2019, 8AM-4PM)
Regression model based on Earth-Sun distance and total ozone column (Sudhibrabha et al. (2006))	7	25.57	25.07
	14	26.10	25.11
	21	26.53	25.45
	28	26.37	25.53
CNN-LSTM-SG-7 Forecast Specific Date	7	16.18 ± 0.42	16.68 ± 0.59
	14	16.09 ± 1.70	16.60 ± 1.77
	21	14.91 ± 1.08	15.24 ± 0.29
	28	14.76 ± 1.39	15.09 ± 1.56
CNN-LSTM-SG-7 Auto-Regressive	7	18.56 ± 2.65	17.41 ± 2.70
	14	20.60 ± 2.31	19.49 ± 2.92
	21	22.51 ± 1.97	21.37 ± 1.83
	28	24.45 ± 1.60	22.62 ± 0.98
CNN-LSTM-SG-14 Forecast Specific Date	7	16.69 ± 0.92	16.73 ± 1.16
	14	14.82 ± 0.63	15.49 ± 1.43
	21	15.96 ± 0.99	16.18 ± 0.46
	28	15.46 ± 0.71	15.55 ± 1.14
CNN-LSTM-SG-14 Auto-Regressive	7	17.31 ± 0.45	17.77 ± 0.55
	14	17.20 ± 0.47	19.16 ± 0.65
	21	17.13 ± 0.50	20.71 ± 0.57
	28	17.00 ± 0.50	20.83 ± 0.97
Seq2Seq-14 (SurfUVNet) Forecast Specific Date	7	12.21 ± 0.65	12.68 ± 0.53
	14	16.42 ± 1.40	12.80 ± 1.64
	21	16.61 ± 1.29	11.97 ± 0.88
	28	18.28 ± 1.57	11.46 ± 0.38
Seq2Seq-14 (SurfUVNet) Auto-Regressive	7	13.13 ± 0.41	13.86 ± 0.91
	14	14.03 ± 0.62	14.09 ± 1.49
	21	14.22 ± 0.74	13.83 ± 2.20
	28	15.79 ± 1.90	13.70 ± 2.65

Table 5.3: Mean absolute percentage errors (MAPE) for long-term antipsoriatic irradiance forecasting for up to 28 days into the future on Nakhon Pathom dataset.

Chapter VI

DISCUSSION

This chapter was taken from our manuscript which has been published (Raksasat et al., 2021).

We have developed SurfUVNet, an artificial neural network model for predicting surface UV radiation that achieves around 10% error for next-day forecast and 13 – 16% error for 7-day up to 4-week forecast. This affirms that quantitative UV forecast is appropriate for heliotherapy applications, which tolerate up to 10 – 25% error level. SurfUVNet’s performance is competitive on UV data from multiple regions, Thailand, Japan, and England, and on both antipsoriatic and downward irradiance. Hence, SurfUVNet can be adapted for forecasting other useful UV action spectra such as vitamin D production and erythematous UV index as well. In fact, our model can even be trained to forecast antipsoriatic irradiance from input erythemally-weighted UV data from a UV Biometer instrument with a small performance reduction (data now shown). This capability is necessary for establishing a national heliotherapy network in Thailand because there is only one full-spectrum UV sensor located in the central region of the country while the rest of the country is covered by a network of UV Biometers.

A key limitation of the artificial neural network is that it tends to overfit to the training dataset and does not generalize well to other datasets that come from different distributions. In the context of UV forecasting, this dictates that the model must be retrained with data from particular weather station in order to be usable for that geographic region. Indeed, the accuracy of each model varies by 5 – 6% across the three geographical regions, Thailand, Japan, and England and even across 2018 and 2019 in the case of London dataset (Table 5.1 and Table 5.2). For the case of London dataset, comparison of UV profiles between consecutive days in 2019 showed an extremely high average variation of 43.57%. The discrepancy in performance of the regression model based on Earth-Sun distance and total ozone column developed by the

Thai Meteorological Department²² between Nakhon Pathom and ERA5 datasets (25% error on Nakhon Pathom and 16 – 19% error on ERA5⁴¹ datasets) could be attributed to the fact that ERA5 data, which contain more detailed ozone measurements (hourly compared to daily) and were computationally interpolated, are likely to be more easily fitted by regression.

The fact that SurfUVNet’s forecast error only weakly correlates with cloud coverage (Figure 5.4) is unexpected but may be explained by the fact that cloud coverage in Nakhon Pathom exhibits clear seasonal pattern (Figure 4.1b) and that the UV radiation profiles are stable over consecutive days (Table 5.1, MAPE of 13.94-14.58 for previous day model). On a geographical region with highly variable weather condition, such as London in 2019, artificial neural network models’ performance drop significantly (Table 5.2) and the error of SurfUVNet exhibits higher correlation with cloud coverage (Figure 5.4c). Hence, artificial neural network models seem to be able to exploit seasonal weather pattern and day-to-day variation to achieve good performance without relying on explicit cloud coverage information. Also, in ozone and AOD500 forecasting experiment, SurfUVNet achieve low error in ozone (ozone MAPE around 3.00) and high error in AOD500 (AOD500 MAPE around 30.00-60.00). The ozone forecasting result is not surprise due to the fact that the model just has to predict one value in all time range. However, SurfUVNet seems to have problem in AOD500 forecasting. It is possible that model can not learn the relationship between AOD500 and UV pattern. This capability of the model to extract seasonal patterns may also explain why addition of ozone and AOD500 information did not improve the performance of SurfUVNet (Figure 5.5), particularly as AOD500 level at Nakhon Pathom closely follows the same seasonal pattern as cloud coverage (Figure 4.1d).

We explored two approaches for forecasting long-term UV radiation. Initially, we expected that developing a specific model for making the forecast for a specific date a certain number of days into the future would yield better performance than an autoregressive approach which use the next-day forecast as input for making the forecast for the day after because forecasting errors would aggregate through autoregressive steps.

However, the models for specific date seem to overfit the training data, performing well on the 2019 dataset but poorly on the 2018 dataset (Table 5.3, 11.46% versus 18.28% error for forecasting up to 28 days into the future). In contrast, the autoregressive approach performs consistently well on both datasets (13.70% and 15.79% error). An explanation for the overfitting of the model trained for specific date maybe because the relationship between today's and next week's UV radiation profiles is so weak that the models learn mostly patterns that are specific to the training dataset. The poor performance of models for multi-day forecast (29.49 – 49.69% error for 7-day forecast) is likely due to the sheer number of outputs that the models must optimize. To make a 7-day forecast at 10-minute resolution, the model has to contain 595 outputs. From these results, we recommend the autoregressive approach for making long-term UV forecast with SurfUVNet.

To prospectively examine whether SurfUVNet's performance is sufficient for heliotherapy applications, we asked photodermatologist at King Chulalongkorn Memorial Hospital to plan a 3-month sunbathing course based on SurfUVNet's output and then compared their schedule with the ground truth antipsoriatic irradiances of the same time interval. This reveals that the error in antipsoriatic dose that the patient would receive by following the clinician's sunbathing protocol remains well within the acceptable 10 – 25% up to 0.3 cloud coverage (Figure 5.4d, MAPE of 11.23). A possible solution for accounting for weather effects on UV radiation that we are exploring is to have each patient carry a portable UV sensor or a smartphone equipped with light sensor and use that data to adjust SurfUVNet's forecast in real-time.

Chapter VII

CONCLUSION

7.1 Summary

In this thesis, we explored and improved UV forecasting model for use in clinical applications. This research is motivated by the low performance of existing UV forecasting models and the fact that many tools require additional weather data such as ozone, AOD, cloud coverage, or humidity. This data requirement limits the usability of the model when applied to different geographical regions. Therefore, we proposed SurfUVNet, a sequence-to-sequence deep learning model that requires only past UV data and has an acceptable error (10-25% MAPE) according to expert photodermatologists.

Like other sequence-to-sequence models, SurfUVNet consists of an encoder and a decoder. SurfUVNet was trained using only UV data and we found that adding more weather data, such as AOD500 or ozone, actually reduced model performance. Unlike previous approaches which trained models using short-term (less than 1-year) data, SurfUVNet is able to learn the annual seasonal pattern of UV and predict future UV profile using information from the same time period of previous year. Our design makes the model aware of annual cycle by encoding date information with a circular index. Overall, SurfUVNet achieves good performance of 10% error for 24-hour forecast and 13-16% error for 7-day up to 4-week forecast in the Nakhon Pathom dataset. SurfUVNet also achieves around 12-13% and 12-18% errors when applying to data from Tokyo, Japan, and London, England, respectively.

7.2 Future work

7.2.1 Adding attention mechanism to the model

In recent works on time series tasks, attention mechanism has proven to be a significant factor that enhances the performance of sequence model (Vaswani et al., 2017). Hence, it is likely that adding an attention mechanism or adapting the encoder

part of a Transformer architecture (Vaswani et al., 2017) will further improve SurfUVNet performance. However, as there are many possible attention mechanisms for sequence-to-sequence model architecture, it may take a long time to find a suitable option and fine-tune the model.

7.2.2 Improving prediction for days with irregular UV profiles

Our experiments have shown that SurfUVNet performs very well when the target day's UV profile resembles the bell-curve pattern, such as days during the Jan-Mar and Oct-Dec periods in Thailand. We reasoned that because the patients are unlikely to sunbath when it is raining or very cloudy, it is acceptable for the model to perform well on days with relatively good weather conditions. However, for general UV forecasting application, the model would be expected to provide decent performance regardless of the weather condition. This limitation may be addressed by either changing model architecture, training separate models to handle different weather conditions, or incorporating real-time weather data such as satellite images to let the model adjust its predictions.

REFERENCES

- Allaart, M., van Weele, M., Fortuin, P., and Kelder, H. 2006. An empirical model to predict the uv-index based on solar zenith angles and total ozone. Meteorological Applications 11 (12 2006): 59 – 65.
- Alpert, J. S. 2015. The jeremiah metzger lecture: Jeremiah metzger and the era of heliotherapy.. Transactions of the American Clinical and Climatological Association 126 (2015):
- Buchholz, W. 1969. [heliotherapy of psoriasis]. Zeitschrift fur Haut- und Geschlechtskrankheiten 44 (1969):
- Buntoung, S., Choosri, P., Dechley, A., Masiri, I., R.Wattan, and Janjai, S. 2012. An investigation of total solar ultraviolet radiation at nakhon pathom, thailand. Procedia Engineering 32 (2012): 427 – 432.
- Cho, K., van Merrienboer, B., Gülçehre, Ç., Bougares, F., Schwenk, H., and Bengio, Y. 2014. Learning phrase representations using RNN encoder-decoder for statistical machine translation. CoRR abs/1406.1078 (2014):
- Deo, R., Downs, N., Parisi, A., Adamowski, J., and Quilty, J. 2017. Very short-term reactive forecasting of the solar ultraviolet index using an extreme learning machine integrated with the solar zenith angle. Environmental research 155 (02 2017): 141–166.
- Elman, J. L. 1990. Finding structure in time. Cognitive Science 14.2 (1990): 179 – 211.
- Elminir, H., Own, H., Azzam, Y., and Riad, A. e.-d. 2008. Testing the applicability of artificial intelligence techniques to the subject of erythematous ultraviolet solar radiation. part two: An intelligent system based on multi-classifier technique. Journal of photochemistry and photobiology. B, Biology 90 (04 2008): 198–206.
- Feister, U., Laschewski, G., and Grewe, R.-D. 2011. Uv index forecasts and measurements of health-effective radiation. Journal of Photochemistry and Photobiology B: Biology 102.1 (2011): 55–68.

- Fischer, T., Alsins, J., and Berne, B. 1984. Ultraviolet-action spectrum and evaluation of ultraviolet lamps for psoriasis healing. International Journal of Dermatology 23.10 (1984): 633–637.
- Foyo-Moreno, I., Vida Manzano, J., and Arboledas, L. 1999. A simple all weather model to estimate ultraviolet solar radiation (290–385 nm). Journal of Applied Meteorology 38 (07 1999): 1020–1026.
- Gardiner, C. F. 1915. Heliotherapy in colorado.. Transactions of the American Climatological and Clinical Association. American Climatological and Clinical Association 31 (1915):
- Gensler, A., Henze, J., Sick, B., and Raabe, N. 2016. Deep learning for solar power forecasting — an approach using autoencoder and lstm neural networks. (2016): 002858–002865.
- Hersbach, H., Bell, B., Berrisford, P., Biavat, G., Horányi, A., J., M. S., Nicolas, J., Peubey, C., Radu, R., Rozum, I., Schepers, D., Simmons, A., Soci, C., Dee, D., Thépaut, and J-N. 2018. ERA5 hourly data on single levels from 1979 to present. copernicus climate change service (c3s) climate data store (cds). (accessed on 30/12/2020). (2018):
- Hitomi, K., Yukinori, K., Takayoshi, H., Hiroyuki, I., Yuko, A., and Angela, S. 2017. Climatotherapy in japan: a pilot study. International Journal of Biometeorology 61 (2017):
- Hochreiter, S. and Schmidhuber, J. 1997. Long short-term memory. Neural Computation 9.8 (1997): 1735–1780.
- Huang, X., Shi, J., Gao, B., Tai, Y., Chen, Z., and Zhang, J. 2019. Forecasting hourly solar irradiance using hybrid wavelet transformation and elman model in smart grid. IEEE Access 7 (2019): 139909–139923.
- Husein, M. and Chung. 2019. Day-ahead solar irradiance forecasting for microgrids using a long short-term memory recurrent neural network: A deep learning approach. Energies 12 (05 2019): 1856.

- Jacovides, C., Tymvios, F., Boland, J., and Tsitouri, M. 2015. Artificial neural network models for estimating daily solar global uv, par and broadband radiant fluxes in an eastern mediterranean site. Atmospheric Research 152 (01 2015): 138–145.
- Janjai, S., Buntung, S., Wattan, R., and Masiri, I. 2010. Mapping solar ultraviolet radiation from satellite data in a tropical environment. Remote Sensing of Environment 114.3 (2010): 682 – 691.
- Kingma, D. and Ba, J. 2014. Adam: A method for stochastic optimization. International Conference on Learning Representations (12 2014):
- Koenker, R. and Hallock, K. F. 2001. Quantile regression. Journal of Economic Perspectives 15.4 (December 2001): 143–156.
- Krzyściń, J. W., Jarosławski, J., Rajewska-Więch, B., Sobolewski, P. S., Narbutt, J., Lesiak, A., and Pawlaczyk, M. 2012. Effectiveness of heliotherapy for psoriasis clearance in low and mid-latitudinal regions: A theoretical approach. Journal of Photochemistry and Photobiology B: Biology 115 (2012):
- Krzyściń, J. W., Narbutt, J., Lesiak, A., Jarosławski, J., Sobolewski, P., Rajewska-Więch, B., Szkop, A., Wink, J., and Czerwińska, A. 2014. Perspectives of the antipsoriatic heliotherapy in poland. Journal of Photochemistry and Photobiology B: Biology 140 (2014):
- Krzyściń, J., Guzikowski, J., Czerwińska, A., Lesiak, A., Narbutt, J., Jarosławski, J., Sobolewski, P., Rajewska-Więch, B., and Wink, J. 2015. 24 hour forecast of the surface uv for the antipsoriatic heliotherapy in poland. Journal of Photochemistry and Photobiology B: Biology 148 (2015):
- Körbler, J. 1967. [to the history of development of heliotherapy]. Hippokrates 38 (1967):
- Leccese, F., Salvadori, G., Lista, D., and Burattini, C. 2018. Outdoor workers exposed to uv radiation: Comparison of uv index forecasting methods. (2018):
- Lecun, Y., Bottou, L., Bengio, Y., and Haffner, P. 1998. Gradient-based learning applied to document recognition. Proceedings of the IEEE 86 (12 1998): 2278 – 2324.

- Legat, F. J. 2018. [importance of phototherapy in the treatment of chronic pruritus]. Der Hautarzt 69 (2018):
- Linsler, K. and Harnack, K. 1962. [heliotherapy of mycosis fungoides]. Arch Klin Exp Dermatol 215 (1962):
- Menter, A., Korman, N. J., Elmets, C. A., Feldman, S. R., Gelfand, J. M., Gordon, K. B., Gottlieb, A., Koo, J. Y., Lebwohl, M., Lim, H. W., Van Voorhees, A. S., Beutner, K. R., and Bhushan, R. 2010. Guidelines of care for the management of psoriasis and psoriatic arthritis: Section 5. guidelines of care for the treatment of psoriasis with phototherapy and photochemotherapy. Journal of the American Academy of Dermatology 62 (2010):
- Metzger, J. 1926. The clinical application of heliotherapy.. Transactions of the American Climatological and Clinical Association. American Climatological and Clinical Association 42 (1926):
- Moosa, Y. and Esterhuysen, D. 2010. Heliotherapy: A south african perspective. South African Medical Journal 100 (2010):
- Nast, A., Spuls, P., van der Kraaij, G., Gisondi, P., Paul, C., Ormerod, A., Saiag, P., Smith, C., Dauden, E., de Jong, E., Feist, E., Jobling, R., Maccarone, M., Mrowietz, U., Papp, K., Reich, K., Rossumeck, S., Talme, T., Thio, H., van de Kerkhof, P., Werner, R., and Dressler, C. 2017. European s3-guideline on the systemic treatment of psoriasis vulgaris – update apremilast and secukinumab – edf in cooperation with eadv and ipc. Journal of the European Academy of Dermatology and Venereology 31.12 (2017): 1951–1963.
- Parrish, J. A. and Jaenicke, K. F. 1981. Action spectrum for phototherapy of psoriasis. Journal of Investigative Dermatology 76.5 (1981): 359 – 362.
- Patrizi, A., Raone, B., and Ravaioli, G. M. 2017. Safety and efficacy of phototherapy in the management of eczema. (2017):
- Qing, X. and Niu, Y. 2018. Hourly day-ahead solar irradiance prediction using weather forecasts by lstm. Energy 148 (2018):

- Raksasat, R., Sri-iesaranusorn, P., Pemcharoen, J., Laiwarin, P., Buntoung, S., Janjai, S., Boontaveeyuwat, E., Asawanonda, P., Sriswasdi, S., and Chuangsuwanich, E. 2021. Accurate surface ultraviolet radiation forecasting for clinical applications with deep neural network. Scientific Reports 11.1 (Mar 2021): 5031.
- Rumelhart, D. E., Hinton, G. E., and Williams, R. J. 1986. Learning internal representations by error propagation. (1986): 318–362.
- Savitzky, A. and Golay, M. J. E. 1964. Smoothing and differentiation of data by simplified least squares procedures.. Analytical Chemistry 36.8 (1964): 1627–1639.
- Schuster, M. and Paliwal, K. K. 1997. Bidirectional recurrent neural networks. IEEE Transactions on Signal Processing 45.11 (1997): 2673–2681.
- Siami-Namini, S. and Namin, A. S. 2018. Forecasting economics and financial time series: ARIMA vs. LSTM. CoRR abs/1803.06386 (2018):
- Snellman, E. 1992. Comparison of the antipsoriatic efficacy of heliotherapy and ultraviolet b: a cross-over study.. Photodermatology, photoimmunology & photomedicine 9 (1992):
- Snellman, E., Jansen, C., Lauharanta, J., and Kolari, P. 1992. Solar ultraviolet (uv) radiation and uv doses received by patients during four-week climate therapy periods in the canary islands.. Photodermatology, photoimmunology & photomedicine 9 (1992):
- Snellman, E., Aromaa, A., Jansén, C. T., Lauharanta, J., Reunanen, A., Jyrkinen-Pakkasvirta, T., Luoma, J., and Waal, J. 1993a. Supervised four-week heliotherapy alleviates the long-term course of psoriasis.. Acta Derm Venereol. 73 (1993):
- Snellman, E., Lauharanta, J., Reunanen, A., JANSEN, C., PAKKASVIRTA, T., KALLIO, M., LUOMA, J., AROMAA, A., and WAAL, J. 1993b. Effect of heliotherapy on skin and joint symptoms in psoriasis: a 6-month follow-up study. British Journal of Dermatology 128 (1993):

- Srivastava, N., Hinton, G., Krizhevsky, A., Sutskever, I., and Salakhutdinov, R. 2014. Dropout: A simple way to prevent neural networks from overfitting. Journal of Machine Learning Research 15.56 (2014): 1929–1958.
- Sudhibrabha, S., Harold, R., Exell, B., and Sukawat, D. 2006. Ultraviolet forecasting in thailand. ScienceAsia 32 (2006):
- Sutskever, I., Vinyals, O., and Le, Q. V. 2014. Sequence to sequence learning with neural networks. (2014):
- Takada, Y., Irisawa, K., and Kawada, A. 1977. Heliotherapy of pityriasis lichenoides chronica. The Journal of Dermatology 4 (1977):
- Vaswani, A., Shazeer, N., Parmar, N., Uszkoreit, J., Jones, L., Gomez, A. N., Kaiser, L., and Polosukhin, I. 2017. Attention is all you need.
- Vinyals, O., Toshev, A., Bengio, S., and Erhan, D. 2014. Show and tell: A neural image caption generator. CoRR abs/1411.4555 (2014):
- Wang, F., Yu, Y., Zhang, Z., Li, J., Zhen, Z., and Li, K. 2018. Wavelet decomposition and convolutional lstm networks based improved deep learning model for solar irradiance forecasting. Applied Sciences 8.8 (2018):
- Zavodska, E. and Reichrt, J. 1985. Ultraviolet and total global radiation in bratislava. Contrib. Slovak Acad. Sci. Ser. Meteorol 5 (1985): 21.

Biography

Name	Raksit Raksasat
DATE OF BIRTH	March 1997
PLACE OF BIRTH	Thailand
INSTITUTIONS ATTENDED	Chulalongkorn University
HOME ADDRESS	439 Soi chaopharayasiam Bangplad Bangkok 10700

